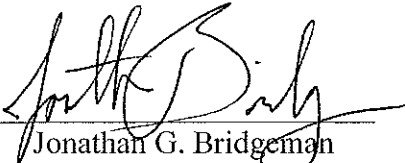UNDERSTANDING MISSISSIPPI DELTA SUBSIDENCE THROUGH

STRATIGRAPHIC AND GEOTECHNICAL ANALYSIS OF A CONTINUOUS

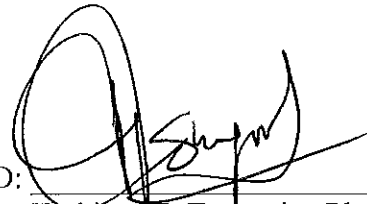HOLOCENE CORE AT A SUBSIDENCE SUPERSTATION

AN ABSTRACT

SUBMITTED ON THE TENTH DAY OF APRIL 2018

TO THE DEPARTMENT OF EARTH AND ENVIRONMENTAL SCIENCES

IN PARTIAL FULFILLMENT OF THE REQUIREMENTS

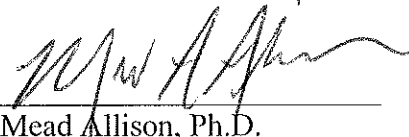OF THE SCHOOL OF SCIENCE AND ENGINEERING

OF TULANE UNIVERSITY

FOR THE DEGREE

OF

MASTERS OF SCIENCE

BY

_____
Jonathan G. Bridgeman

APPROVED: _____
Torbjörn E. Törnqvist, Ph.D.

_____
Mead Allison, Ph.D.

_____
Navid Jafari, Ph.D.

ABSTRACT

Land-surface subsidence can be a major contributor to the relative sea-level rise that is threatening many coastal communities. Loosely constrained subsidence rate estimates across the Mississippi Delta make it difficult to differentiate between subsidence mechanisms and complicate modeling efforts. New data from a nearly 40 m long, 12 cm diameter core taken during the installation of a subsidence monitoring superstation near the Mississippi River, southeast of New Orleans, provides insight into the stratigraphic and geotechnical properties of the Holocene succession at that site. Stratigraphically, the core can be grouped into four units. The top 12 m is dominated by clastic overbank sediment with interspersed organic-rich layers. The middle section, 12-35 m, consists predominately of mud, and the bottom section, 35-38.7 m, is marked by a transition into a Holocene-aged basal peat (~11.3 ka) which overlies densely packed Pleistocene sediment. Radiocarbon and OSL ages are used to calculate vertical displacement and averages subsidence rates as far back as ~3.5 ka, yielding values as high as 8.0 m of vertical displacement (up to 2.34 mm/yr) as obtained from a transition from mouth bar to overbank deposits. We infer that most of this was due to compaction of the thick, underlying mud package. The top ~80 cm of the core is a peat that represents the modern marsh surface and is inducing minimal surface loading. This is consistent with the negligible shallow subsidence rate as seen at a nearby rod-surface elevation table – marker horizon station. Future compaction scenarios for the superstation can be modeled from the stratigraphic and geotechnical properties of the core, including the loading from the planned Mid-Barataria sediment diversion which is expected to dramatically change the coastal landscape in this region.

UNDERSTANDING MISSISSIPPI DELTA SUBSIDENCE THROUGH

STRATIGRAPHIC AND GEOTECHNICAL ANALYSIS OF A CONTINUOUS

HOLOCENE CORE AT A SUBSIDENCE SUPERSTATION

A THESIS

SUBMITTED ON THE TENTH DAY OF APRIL 2018

TO THE DEPARTMENT OF EARTH AND ENVIRONMENTAL SCIENCES

IN PARTIAL FULFILLMENT OF THE REQUIREMENTS
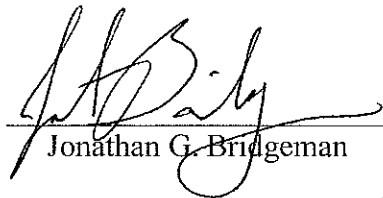
OF THE SCHOOL OF SCIENCE AND ENGINEERING

OF TULANE UNIVERSITY

FOR THE DEGREE

OF

MASTERS OF SCIENCE

BY

_____
Jonathan G. Bridgeman
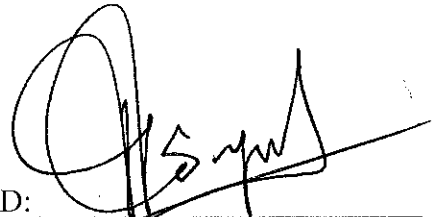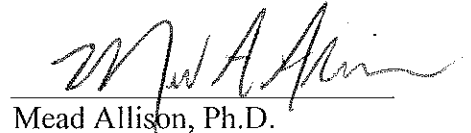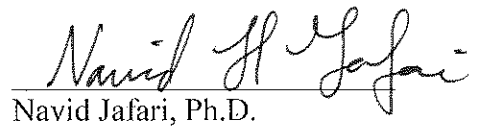
APPROVED: _____
Torbjörn E. Törnqvist, Ph.D.

_____
Mead Allison, Ph.D.

_____
Navid Jafari, Ph.D.

ProQuest Number: 10789629

ProQuest 10789629

Published by ProQuest LLC (2018). Copyright of the Dissertation is held by the Author.

ProQuest LLC.
789 East Eisenhower Parkway
P.O. Box 1346
Ann Arbor, MI 48106 – 1346

ACKNOWLEDGEMENTS

Matthew 7:24-27

TABLE OF CONTENTS

LIST OF TABLES

LIST OF FIGURES

1.   INTRODUCTION

Restoration of the Mississippi River Delta (MRD) is a multi-billion dollar effort to counteract coastal Louisiana's severe land loss which is primarily caused by eustatic sea-level rise, land subsidence, and a lack of new sediment (Couvillion et al., 2011; LCPRA, 2017). Subsidence, the focus of this study, is a complex process that varies both temporally and spatially across the MRD. It consists of multiple drivers, with different magnitudes, which can produce rates up to 65 mm/yr (Jankowski et al., 2017). Quantifying the effects of these drivers is subject to much debate but is critical to the efforts to slow land loss and restore the MRD. Currently, subsidence maps can have uncertainties of over 3 cm/yr (e.g., LCPRA, 2017) which creates a wide range of possible outcomes for restoration projects and convolutes both planning and management strategies.

The MRD started to take its current form during the second half of the Holocene. During the mid-Holocene, rates of sea-level rise slowed and the MRD started to prograde and build the first of the subdeltas still recognizable in the landscape. Alluvial deposition, or accretion, was dominant in the active subdeltas which offset submergence from sea-level rise and subsidence. As the river switched its course within the delta it built a new subdelta while the previous subdelta began to decay. Therefore, within the natural delta plain, there was always a mesh of growing and declining portions (Roberts, 1997). Recently, human management, along with sea-level rise, has changed this delta cycle. Erosion rates have increased due to new pipeline and navigation channels, whereas artificial levees have decreased overbank flow of sediment onto the delta plain, stymieing accretion. Additionally, upstream dams have trapped up to 50% of the Mississippi River's

historic sediment load (Kesel et al., 1992). This has led to a sediment starved delta that is rapidly losing land.

In the MRD, subsidence is controlled by multiple drivers ranging from sub-mm/yr to as high as a couple of cm/yr (Blum and Roberts, 2012) (Fig. 1). While the exact magnitude of integrated and driver-specific rates is often disputed, glacial isostatic adjustment (Wolstencroft et al., 2014), growth faults (Dokka, 2011; Armstrong et al., 2014), and sediment compaction (Meckel et al., 2006; Törnqvist et al., 2008) have all been argued to be important drivers.
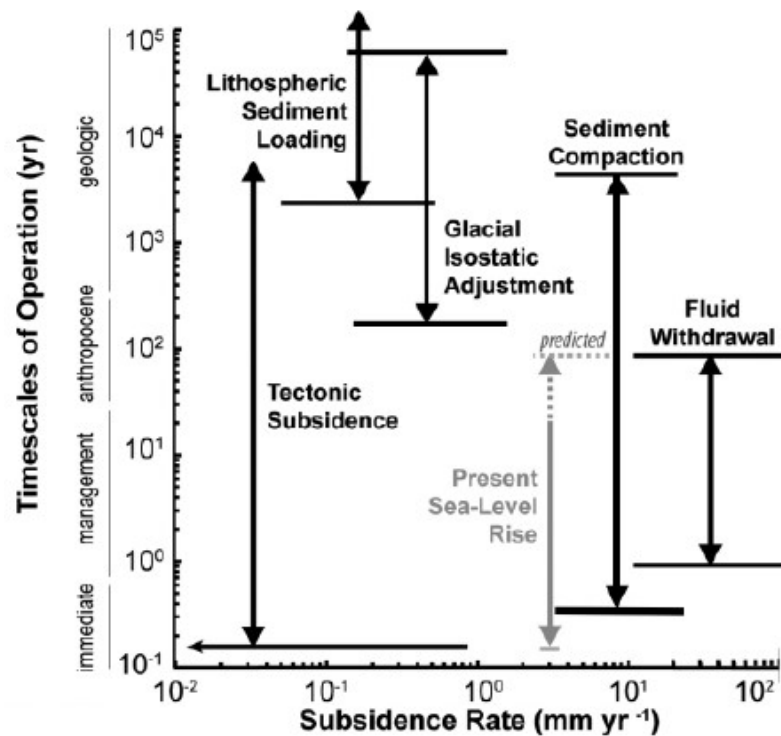
Figure 1 *Rates and time scales of subsidence mechanisms in coastal Louisiana. Predicted eustatic sea-level rise is included with possible range represented by a dotted line. Figure from Allison et al. (2016).*

Other drivers like salt tectonics and sediment isostatic adjustment play only minor roles in the MRD (Peel et al., 1995; Yu et al., 2012; Wolstencroft et al., 2014). Over the last century, particularly in the 1960s and 1970s, natural subsidence accelerated due to the extraction of millions of barrels of hydrocarbons from the MRD (Morton and Bernier, 2010; Kolker et al., 2011). Rates continued to increase after oil production moved offshore due to continued shale compaction but have since returned to background levels (Chang et al., 2014). In addition to hydrocarbons, groundwater extraction has also induced subsidence, albeit mainly in urban and industrial areas (Jones et al., 2016). Despite these occasional high rates of subsidence due to deep subsidence processes, published data suggest that shallow subsidence (i.e., compaction within the Holocene sediment package) is contributing most to the observed rates (Törnqvist et al., 2008; Jankowski et al., 2017). The importance of quantifying these rates is evident in Louisiana's efforts to counteract coastal land loss with the numerous projects proposed in the $50 billion Coastal Protection and Restoration Authority's (CPRA) 2017 Louisiana's Comprehensive Master Plan (CMP) for a Sustainable Coast (LCPRA, 2017). In order to maximize land building efforts, subsidence must be correctly attributed to the rates and spatial trends of the drivers.

In order to better understand the interplay of various subsidence drivers acting at specific depths, and, ultimately, to predict subsidence rates, we chose an experimental field site in a brackish marsh in the Plaquemines-Modern subdelta just south of Belle Chasse, Louisiana (Fig. 2). The field site is 2 km from the Mississippi River, 170 m from Coastal Reference Monitoring (CRMS) site 0276 which provides an established reference point for subsidence over the last 10 years, and 5 km south of the proposed Mid-Barataria sediment diversion, one of the CMP's primary targets to build new land in the MRD (Fig. 2). A 38.7

m continuous sediment core from this field site was analyzed to study compaction rates

over the Holocene and to quantify the shallow subsurface component of subsidence.
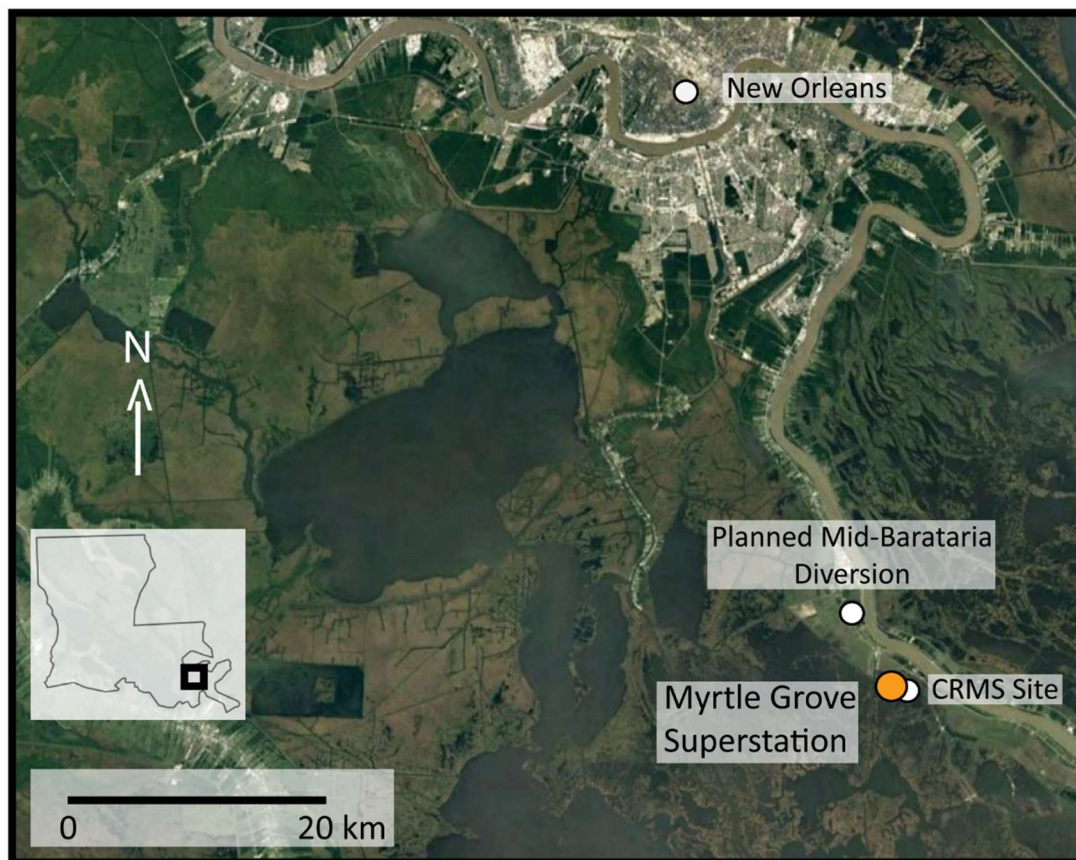
Figure 2 *The field site is located in a brackish marsh near the Myrtle Grove Marina in Plaquemines Parish, Louisiana. It is 5 km south of the planned Mid-Barataria sediment diversion and 170 m from CRMS site 276 which uses a rod surface-elevation table-marker horizon system to determine surface-elevation change, vertical accretion, and shallow subsidence rates.*

2.   STUDY CONTEXT

The Plaquemines-Modern subdelta became active 1.0-1.4 ka (where ka is relative to 2010 CE) (Hijma et al., 2017). Of the five lobes in the MRD (Fig. 3), the Plaquemines-Modern is one of only two currently active subdeltas. Because the river is fully embanked, the delta plain is cut off from the Mississippi River's direct water and sediment supply. In the region, low lying artificial levees were built along the banks as early as 1888 but where not raised to federal standards until 1928 with the implementation of the Mississippi River & Tributary levees (Plaquemines Parish, 2014). A locally funded back-levee was built ~1 km from the MR&T levees and while the date of construction is unclear, it was likely after 1928 due to inclusion of riprap in its construction. With this lack of sediment input, CRMS stations from the Mississippi Delta show that 35% of wetlands are vulnerable to submergence because they are accreting sediment (mineral + organic) at too low a rate (Jankowski et al., 2017), although this is not the case for the closest CRMS site (0276), 170 m from our site. The rod surface-elevation table-marker horizon data show a marsh accretion rate of 14.4 mm/yr, which is mostly organic accretion, whereas the total subsidence rate is 4.6 mm/yr at CRMS 0276. However, the shallow subsidence component of this rate (measured from the land surface to 26.5 m depth) is only 0.4 mm/yr (Jankowski et al., 2017). While current subsidence and accretion rates at the Myrtle Grove site may not be representative of the MRD as a whole, the underlying subsidence mechanisms affecting the site are the same.

The analysis and description of the Myrtle Grove I sediment core is part of a larger project known as the Myrtle Grove Subsidence Superstation (henceforth "Superstation") (Fig. 2 and 3). The Superstation is an interdisciplinary effort that uses multiple techniques

to study the depth and temporal variability of subsidence (Allison et al., 2016). By integrating different measurement techniques at one location, the magnitude of deep and shallow subsurface processes can be accurately constrained. It should be noted that this study defines shallow subsidence as occurring within the Holocene sediment column.
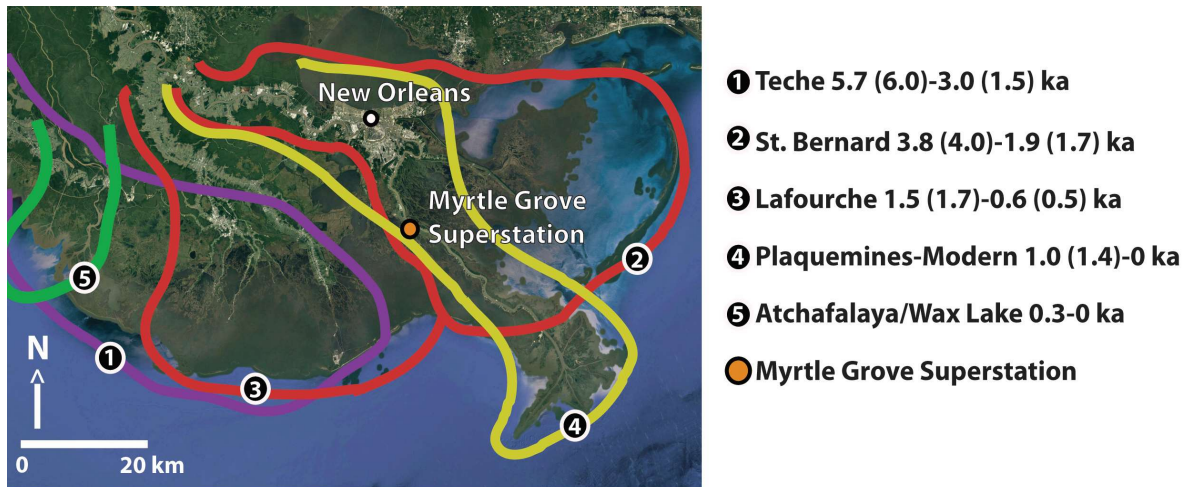
Figure 3 The Myrtle Grove Superstation with respect to the five Mississippi River Delta subdeltas. Ages listed are the period of activity with the ages in parentheses indicating the possible period of activity. Modified from Roberts (1997); Blum and Roberts (2012); Hijma et al. (2017)

At the Superstation there are three wells: well 1 (38.7 m deep), well 2 (25 m), and well 3 (10 m) (Fig. 4). Each well contains a fiberoptic strainmeter and a GPS station. The strainmeters will highlight any variations in shallow subsidence that occur within the Holocene succession, with well 3 measuring the top 10 m, well 2 measuring the top 25 m, and well 1 measuring the entire Holocene succession (~37.8 m). The GPS stations will record subsidence at a depth of 3 m, except for well 1 which measures subsidence at the base of the deep well. This means that the GPS station at well 1 measures deep subsidence, or displacement occurring below the Pleistocene-Holocene transition and wells 2 and 3 measure deep subsidence plus a large portion (in terms of depth) of shallow subsidence.

Subsidence occurring within the top 3 m, potentially a large portion of shallow subsidence, is not measured in any of the wells because the instrumentation is housed in 3 m long metal casings near the surface. Installation of the electronic equipment was completed over several months: two strainmeters (well 1 and 3) in July 2016, three GPS stations (well 1, 2, and 3) in August 2016, and the third strainmeter (well 2) in May 2017.
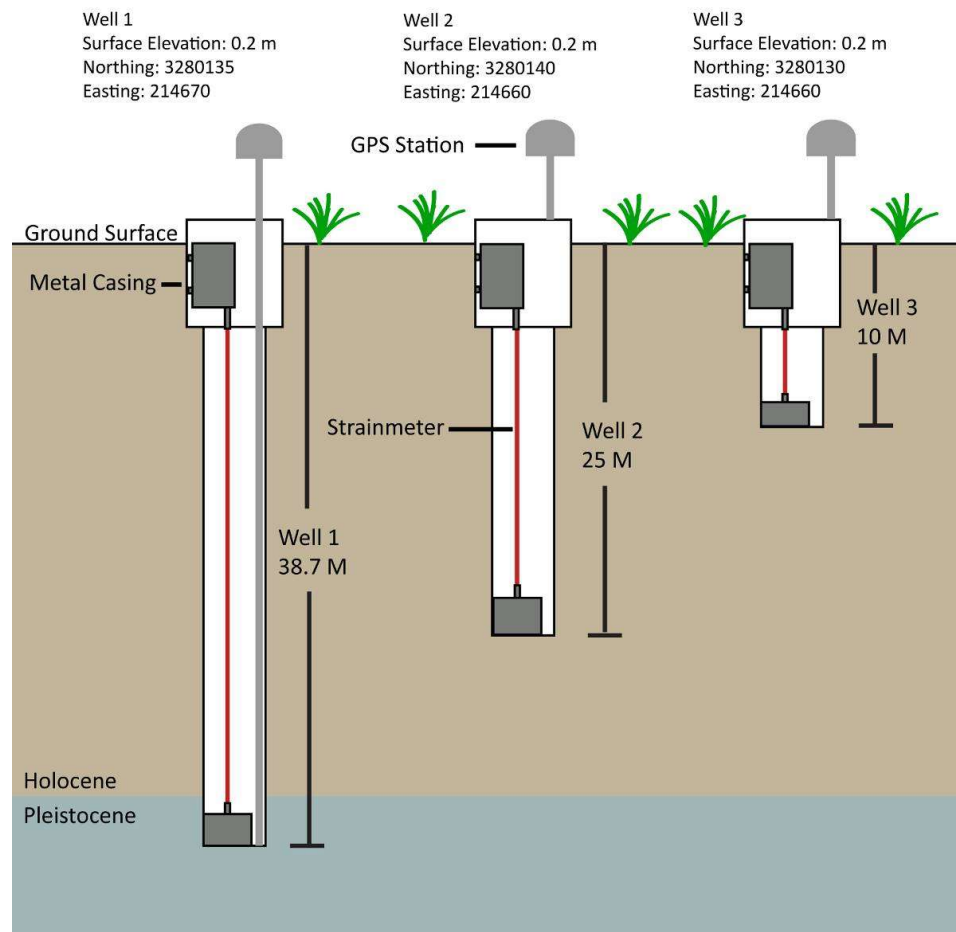
Figure 4 *Myrtle Grove Superstation instrumentation to measure subsidence over three different depth intervals. Coordinates are reported in UTM 16N.*

While the Superstation measures active subsidence rates, stratigraphic analysis of the 38.7 m core collected at the site provides insight into the Holocene subsidence history which will complement shallow subsidence rates measured at the Superstation and nearby

CRMS site 0276. Additionally, the analysis will provide a better understanding of which facies are most prone to compaction and help quantify the role of compaction at the Superstation. This is particularly relevant because a better understanding of compaction will provide valuable insight into the management of the planned Mid-Barataria sediment diversion, 5 km upriver, and allow for comparison of subsidence rates before and after the diversion becomes operational. If this sediment diversion is successful, it will pave the way for more diversions which could build a significant amount of new coastal land and reduce wetland loss in the region. Therefore, I seek to test the following hypothesis:

Holocene subsidence rates at the Myrtle Grove Superstation were controlled primarily by sediment compaction, an active shallow subsurface process.

Within the scope of the larger Superstation project, I will develop a detailed understanding of the sediment and geotechnical properties at the field site. These characteristics can elucidate which depth intervals at the Superstation are most prone to subsidence, which will help interpret the instrumental records and to potentially decipher the role of multiple subsidence drivers that may be active at the site.

To test this hypothesis and to achieve the larger goals of this thesis, I will complete the following objectives:

- *Identify sedimentary facies and grain size of the 38.7 m long core.*
- *Measure geotechnical sediment properties of the core.*
- *Quantify vertical displacement rates of organic-rich and sandy intervals within the core.*

3.   METHODS

3.1   *Core Collection and Storage*

3.1.1   *Core Collection*

The 38.7 m long core was collected at the Superstation site (Fig. 2) in January 2016 by Fugro, an international geotechnical firm. It was recovered in 1.22 m long increments with a 12.7 cm diameter piston corer on top of a ~10 m long marsh buggy. The first drive was an exception and only reached 0.91 m as dictated by drilling protocol. After drilling, the core segments were stored vertically at room temperature for several days in a warehouse at Fugro's Kenner, Louisiana, office.

3.1.2   *Initial Description and Storage*

The sediment was extruded from the aluminum casing of each core interval with a hydraulic pushrod. The outer layer of sediment was cleared away to avoid contamination from sediment migration along the casing walls during drilling and the dominant texture was described in increments of 0.1 m following the U.S. Department of Agriculture (USDA) sediment texture classification system (USDA, 1999) (Fig. 5). Color, organic-matter content, plant remains, and other notable facies characteristics were documented along with sediment texture in the core description. It is important to note that all the described peats may not fit the definitions laid out for engineering purposes, like those found in Mesri and Ajlouni (2007), but are consistent with other studies such as Chamberlain (2017). The core was cut into ~0.25 m core segments and sealed in plastic wrap and aluminum foil. In order to preserve the sediment properties and water content, the core segments were placed in plastic containers and sealed with wax. The core segments were then taken to Tulane University and refrigerated at 2°C in vertical position.

Sediment Textural Triangle
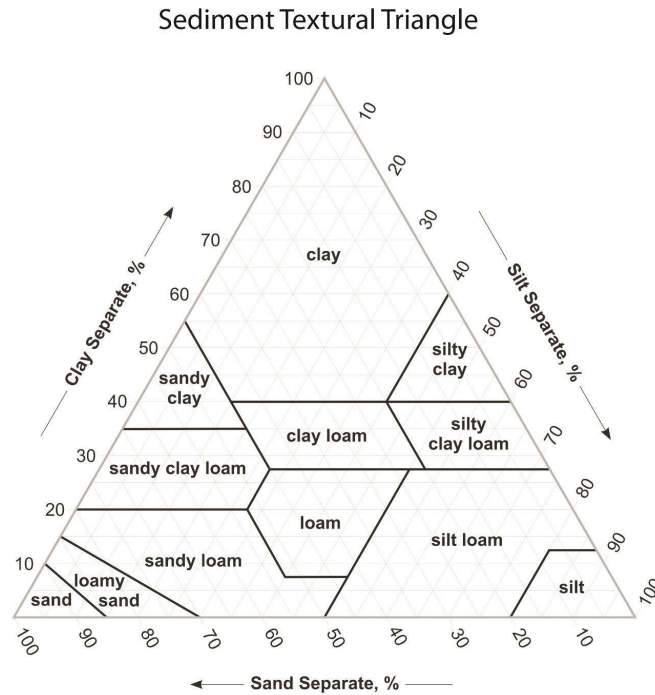
Figure 5 *US Department of Agriculture texture triangle used for describing the sediment texture of the Myrtle Grove I core. Clay-silt and silt-sand boundaries are at 2 and 50 μm, respectively.*

3.1.3   Hand-cored Cross Section

In addition to the Myrtle Grove I core, a cross section was drilled in August of 2017 to determine the shape and extent of several major beds found in the upper portion of the deep core, with the purpose of better understanding the evolution of the study area. Sediment texture was described in 0.1 m depth increments until we reached the delta-front laminations below the sand or we became stuck in a sandy interval. These nine boreholes were drilled with an Edelman hand auger and gouge and all elevations were determined relative to the North American Vertical Datum of 1988 (NAVD 88).

3.2   Laboratory Analysis

3.2.1   Continuous Bulk Density Measurements

In April 2016, prior to removing the wax casings, each section of the long sediment core was scanned with a Geotek Multi-Sensor Core Logger at the College of the Coast and Environment Sediment Laboratory at Louisiana State University using a ^{137}Cs gamma source to obtain a continuous bulk density profile. Calibration parameters to account for the storage container were calculated by an initial scan of a density standard. The wax coated core segments were then scanned at 1 cm intervals with the non-intrusive logger to ensure a high-precision measurement and to preserve core properties for later tests. Resulting raw data were processed with the initial calibration parameters to produce wet bulk density measurements.

3.2.2   Discrete Bulk Density Measurements

Corrections to the in-situ scanned bulk density measurements for moisture content and wax coating were made by means of 138 bulk density measurements at intervals of 5 to 25 cm throughout the core in the Quaternary Research Laboratory at Tulane University. Each described sediment texture was sampled at least once and the results were used as a guide for corrections to the high-resolution wet bulk density scan.

To make the laboratory measurements of bulk density, the outer 2 mm of the core were removed to provide a fresh sampling surface and 3.75 mL samples were collected with a 2 cm diameter, wide-mouth EasyDraw syringe and then extruded into small ceramic crucibles. Samples from the top 8 m of the core were collected with a scoop instead of a syringe because the syringe was unable to sample this relatively unconsolidated material.

These sediments were scooped into the 4.82 mL crucibles and extra care was taken to eliminate air pockets and not to over pack the crucibles. Next, the samples were weighed (W_1), dried at 75°C for 24 hours, and reweighed (W_2). The water content (w_c) was calculated using the following equation:

$$w_c \ (\%) = \left(\frac{W_1 - W_2}{W_1}\right) x \ 100 \qquad\qquad (\ 1\ )$$

Dry bulk density was calculated by dividing each sample's dried weight (W_2) by the sample volume.

The effects of water content and wax coating on the wet bulk density data were corrected with these lab results. Changes were made according to linear relationships between discrete and scanned bulk densities as further explained in Section 4.4.

3.2.3   Loss on Ignition Measurements

Each of the 138 oven-dried samples collected for the discrete bulk density measurements were also measured for loss on ignition (LOI) using the same sampling technique. After desiccation, the samples were powdered, reheated to 75°C, then weighed (W_3) and burned at 550°C for 6-8 hours. After cooling to 75°C, they were weighed a final time (W_4). The organic-matter content was then calculated using the following equation:

$$LOI \ (\%) = \left(\frac{W_3 - W_4}{W_3}\right) x \ 100 \qquad\qquad (\ 2\ )$$

With the exception of the initial weight, samples were always weighed at 75°C to minimize the effects of humidity. This temperature differs slightly from the methodology outlined in Heiri et al. (2001) but additional testing indicated only a 0.1% difference in mass between

drying techniques. Further errors in sample measurements can be attributed to sample size, which could be significant between samples collected with the syringe versus the scoop, or crucible positioning in the furnace (Heiri et al., 2001).

3.2.4 Grain-Size Analysis

Grain-size analysis provides a precise, quantitative check on our qualitative physical description. At least one sample was taken from sediment textures occurring in layers greater than 0.2 m in thickness and at least three samples from those greater than 1 m.

The samples were placed in 250 mL beakers and covered with a deflocculant (sodium metaphosphate). They were then treated with 10% HCl to dissolve carbonates and neutralized with NaOH to a pH of ~7. Fine-grained organic matter was dissolved with H_2O_2 and remnant organic matter was removed with a 250 μm sieve. Grain-size distributions were measured at the Tulane River and Coastal Center with a Malvern Mastersizer 3000, a laser diffraction particle size analyzer, which produced a frequency distribution of grain sizes for each sample. Percentages of sand (50-250 μm), silt (2-50 μm), and clay (0-2 μm) were calculated, plotted, and compared with the physical description. All metrics were calculated using the method of moments by the Malvern software. Additionally, D10, D50, and D90, were also determined by the Malvern software.

3.2.5 Paleo-environmental Analysis

Two different analyses, stable carbon isotope analysis and macrofossil analysis were performed to reconstruct paleo-environments at selected levels in the core. Stable carbon isotope samples were collected from organic-rich materials, treated with HCl to remove carbonates, dried, and powdered following Chmura et al. (1995). They were then

sent to the College of Marine Science at the University of South Florida for analysis where the bulk samples were divided into subsamples of either two or three for each interval. Resulting ^{13}C/^{12}C ratios are expressed as δ^{13}C (in ‰), defined by the following equation:

$$\delta^{13}C = [(^{13}C/^{12}C_{sample})/(^{13}C/^{12}C_{standard}) - 1] \times 10^3 \qquad (3)$$

Plant macrofossil samples, later used for ^{14}C dating, were collected from the three organic-rich layers and sent to Dr. Lee Newsom at Flagler College for identification.

3.2.6 *Compressibility and Permeability*

One-dimensional (1-D) consolidation tests are utilized to measure the decrease in void ratio when subjected to increasing effective vertical stresses (σ'_v). The results provide compressibility and permeability properties that can be incorporated into settlement analyses to estimate the magnitude and rate of settlement in a sediment column. In the Myrtle Grove I core, eight samples were tested: one from the Pleistocene, three throughout the thick mud unit from 12-35 m, and four from the top 10 m. To prepare a 1-D consolidation test in a fixed ring consolidometer, each sample was trimmed to fit into a stainless steel container and subsequently weighed to determine the unit weight and moisture content. The container was placed in a water bath with two porous stones located on the top and bottom to enable drainage (Fig. 6). The first pressure of 12 kPa (250 psf) was applied and the vertical dial gage readings were recorded at preset time intervals (ASTM International, 2017a). When the dial gauge reading was stable for three consecutive time intervals, the load pressure was doubled. This process was repeated to a final pressure of 1,530 kPa (32,000 psf). Testing and post-processing were performed in the Louisiana Transportation Training & Education laboratory at Louisiana State

University by Mr. Brian Harris under the direction of Dr. Navid Jafari. Further details about compressibility and permeability methods are reported in Olson and Daniel (1981).
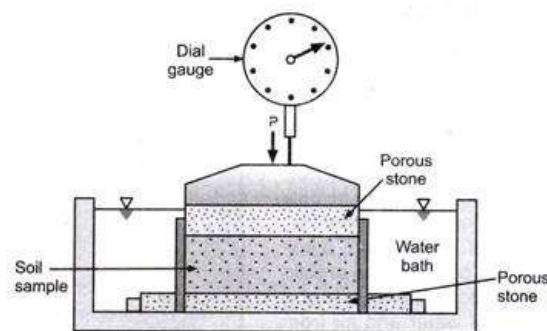
Figure 6 *An example of a fixed ring consolidometer used to measure compressibility and permeability. Image from Das (1990).*

3.3 Geochronology

3.3.1 Radiocarbon Dating

Samples were collected from three organic-rich layers within the core. Two of the organic-rich layers were <0.3 m thick so only one interval was sampled. The third was 0.8 m thick, so intervals at the top and base of the unit were sampled. The samples were wet-sieved with a 250 μm mesh and under magnification, charcoal and seeds were picked, weighed, and stored in vials with water and a small amount of 10% HCl to minimize biological activity. The samples were sent to the Keck-Carbon Cycle Accelerator Mass Spectrometry (UCIAMS) facility at the University of California, Irvine, for measurement. For each interval, two samples were dated to increase accuracy and precision. A weighted mean of the resulting ages for each depth interval was calculated with 1σ errors, then calibrated to calendar ages using OxCal version 4.2 (Bronk Ramsey, 1995). Calibrated radiocarbon ages are expressed relative to 2010 CE.

3.3.2 Optically Stimulated Luminescence Dating

In the summer of 2016, four samples were collected for optically stimulated luminescence (OSL) dating from the Myrtle Grove I borehole. The borehole was hand-drilled immediately adjacent to the site of well 1 and the samples were captured with a stainless steel Eijkelkamp sampler. During collection, samples were handled in such a way that they were not exposed to sunlight. The samples were then taken to a dark room with subdued red light at Tulane University and wet sieved to isolate the 100-250 μm sand fraction. Carbonates were dissolved with a 10% HCl solution which was neutralized with 10% NaOH, and organics were dissolved with 35% H_2O_2. Dose rate measurements were carried out at Tulane University following procedures outlined in Adamiec and Aitken (1998), before the samples were packaged and sent to Wageningen University (The Netherlands) for equivalent dose measurements. Laboratory procedures at Wageningen University are outlined in Appendix A and single-aliquot regeneration (SAR) measurements followed Murray and Wintle (2000). Ages are reported in ka relative to 2010 CE. A complete account of OSL methodology, dose rate estimation, and age calculations is provided in Appendix A which was written with input from E.L. Chamberlain.

4.   RESULTS

4.1   Depth Control

An accurate depth scale for the sediment core is critical to the objectives of this study for several reasons, but the primary reason is because the elevation of dated peats and mouth-bar sands will be matched with a compaction-free relative sea-level curve to calculate vertical displacement.

In terms of uncertainty, we assume that there is negligible error associated with the top and base elevation of each drive. The primary error occurs when there is 1.22 m of penetration but no full recovery. This was the case for every drive, but to varying extents. The "effective recovery", or the length of sediment described, ranged from 0 to 1.13 m but Fugro removed 5 cm from the bottom of each drive to make room for a cap and in the lab, an additional 0-5 cm were removed from the top due to contamination from the drilling mud, so "total recovery" is the effective recovery plus the removed sediment (Table 1). During drive 10 (Table 1), a split spoon sampler was used, instead of a piston core, because the Fugro drillers determined they had reached a relatively thick sand body. This is standard operating procedure for Fugro (Peter Cole, personal communication, July 2016) and the 1.22 m interval was recovered and stored in a small bag. No analysis could be done on this bag sample, so it is recorded as 0 m of recovery.

Total recovery, which is always shorter than the length of the drive, is affected by two factors (Fig. 7). The first is core shortening, which involves the expulsion of air and water from pore spaces, decreasing the distance between sediment grains. As the aluminum liner fills with sediment, shortening leaves a void space near the top of the casing. In general, the shortening is highly variable during drilling and is predominately controlled

by porosity, water, and organic content, as well as sediment texture, but generally decreases with depth (Morton and White, 1997).
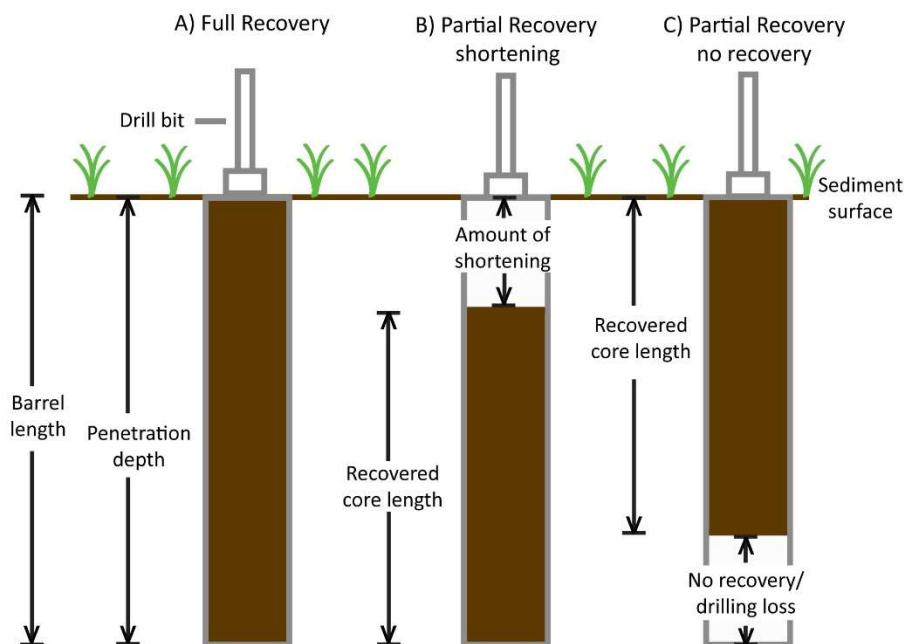
Figure 7 *Examples of core recovery and how it is affected by different confounding processes. A) Full recovery with no disturbance to the core. B) Core recovery in unconsolidated sediment producing shortening within the core barrel. C) Core recovery in more consolidated sediment with a section of no recovery, possibly due to low clay content of the sediment. Modified from Morton and White (1997).*

The second factor is simply no recovery, which occurs when a portion of the cored material does not stick to the sides of the liner, leaving an empty space at the base of the casing. It occurs most commonly with sands that have low clay content but it can occur in all sediment types (Glew et al., 2002). If measurements of gaps at the top and base of the core barrel are conducted immediately after collection, these two factors can be differentiated, but this was not possible because of Fugro's drilling procedures, so the two factors are indistinguishable. There are multiple solutions how address this issue, each of which with its own merits, but percent recovery is used as the main metric. Other methods,

based on geotechnical parameters or water content, do not show clear trends that could be used to determine shortening, whereas total recovery does.

Total recovery (Table 1) starts with low values (71%) in the shallowest part of the Myrtle Grove I core and increases over the next two drives (77 and 94%). It remains at approximately 94% over the next two drives. While recovery is slightly lower for drives 6-8 (84-89%), it is very unlikely that shortening would increase with depth when there is such high recovery for drives 3-5. Furthermore, core shortening is known to occur only in the most compressible sediment in the top few meters (Glew et al., 2002, Kuecher, 1994, Morton and White, 1997). Based on these total recoveries, core shortening is interpreted to occur in the top 2 drives and accounts completely for the differences between full recovery (length drilled) and total recovery. Starting in drive 3, shortening is assumed to have a negligible effect, because total recovery is constant for three consecutive drives. Therefore, remaining sediment gaps are described as sections of no recovery, or sediment loss, which occur at the base of each drive (Fig. 6).

Shortening is corrected separately for each drive and is assumed to occur uniformly within a drive. To calculate shortening, length drilled, $L_{drilled}$, is divided by total recovery, $L_{recovered}$, or

$$Shortening = L_{drilled} / L_{recovered} \qquad\qquad (4)$$

For the first drive, shortening equals 1.40. This means that 1 cm from the first drive is equal to 1.4 cm on a true depth scale. The true depth scale is calculated using the corresponding shortening factor for every centimeter. For the second drive, the shortening

factor is 1.31. For all the other drives, where shortening is assumed to be negligible, a

shortening factor is not required and sediment loss is described as sections of no recovery.

Table 1 *Recovery measurements for each drive. Effective recovery is the amount of sediment described and total recovery, which is used for depth corrections, includes a 5 cm "cap" that was removed in the field and a few additional cm that were removed in the lab (with the exception of drive 10).*

Drive	Core Depth (cm)	Effective Recovery (cm)	Total Recovery (cm)	Length Drilled (cm)	Total Recovery (%)
1	91	60	65	91	71.4
2	213	88	93	122	76.9
3	335	107	114	122	94.2
4	457	105	113	122	93.4
5	579	108	115	122	95.0
6	701	101	107	122	88.4
7	823	96	102	122	84.3
8	944	100	108	122	89.3
9	1066	105	113	122	95.0
10	1188	0	0	122	0.0
11	1310	93	101	122	83.5
12	1432	99	104	122	84.3
13	1554	103	110	122	86.8
14	1676	91	98	122	81.0
15	1798	102	110	122	90.9
16	1920	70	77	122	63.6
17	2042	75	85	122	70.2
18	2164	113	119	122	99.2
19	2286	75	83	122	68.6
20	2407	103	112	122	92.6
21	2529	111	118	122	97.5
22	2651	107	117	122	96.7
23	2773	82	92	122	76.0
24	2895	97	105	122	86.0
25	3017	110	120	122	99.2
26	3139	108	116	122	95.9
27	3261	40	48	122	39.7
28	3383	109	117	122	96.7
29	3505	60	67	122	55.4
30	3627	101	108	122	89.3
31	3749	70	78	122	65.3
32	3871	50	55	122	45.5
Total	**3871**	**2839**	**3077**	**3871**	**79.5**

4.2   Core Description

The 38.7 m long Myrtle Grove I core is composed largely of mud (silt and clay) with a few significant peat and sand beds (Fig. 8). Of the total 38.7 m drilled, 79.5% of the core was recovered (Table 1). The core can be subdivided into four units based on granulometry and sedimentary structures: unit 1 (0-11.9 m), unit 2 (11.9-35.1 m), unit 3 (35.1-37.5 m), and unit 4 (37.5-38.7 m). All depths, both here and in the following sections, are reported as measured from the land surface which is +0.2 m NAVD 88.

Unit 1 is dominated by alternating silty clay loam and silt loam (Fig. 8). The unit is bounded on top by the modern marsh surface, represented by a 0.8 m thick peat bed, and a 1.8 m thick sand body at the base. The unit contains two additional organic-rich beds, a humic clay at a depth of 4.2-4.5 m and an intercalated peat from 6.7-7.5 m depth. Between these two beds, there is a 2.0 m interval of alternating silt loam and sandy loam textures. The base of this 2.0 m interval forms an unconformity with the top of the intercalated peat. Shell fragments were found at both this unconformity and overlying it in a sand layer at a depth of 6.3-6.4 m.

Unit 2 is mud-dominated and much more homogenous than unit 1. The mud is composed of silty clay with mm-scale silt laminations between 12 and 18 m. One distinct feature is located near the base of the unit: a sandy loam from 28.6-28.8 m. The sandy loam is interbedded with silty clay loam and contains shell hash.
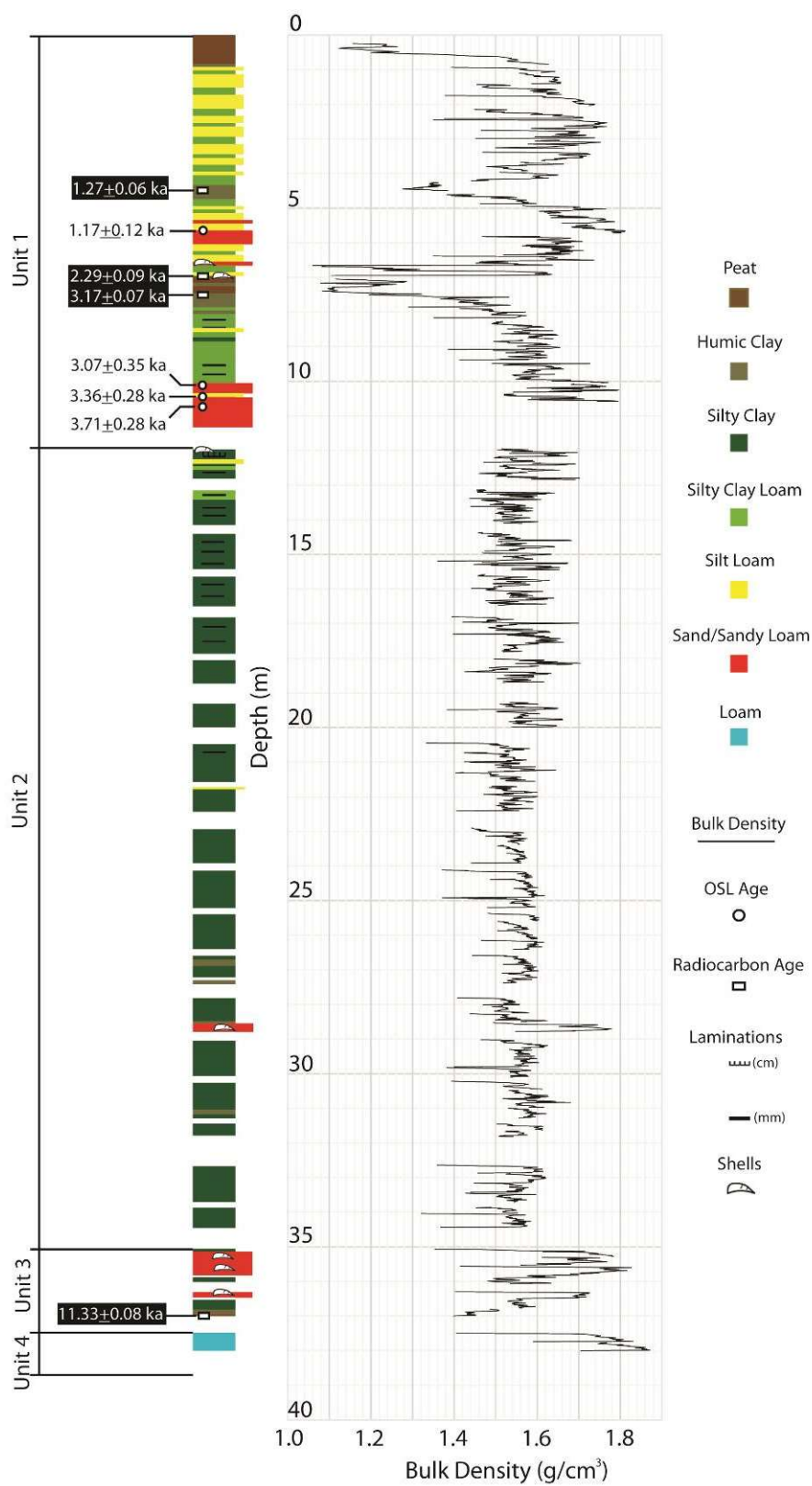
Figure 8 *Sediment description, geochronology, and scanned raw bulk density (which includes the wax casing) for the 38.7 m Myrtle Grove I core.*

Unit 3 can be broken up into two subunits. The first is a 1.1 m thick sand body with shell hash and reworked mud near 35.5 m (Fig. 8). The shell hash contains well-preserved *Rangia* sp. clams, 3 cm in diameter, but consists mostly of shell fragments. Below this sand, there is 0.3 m of silty clay which transitions into a near-basal wood peat bed; this marks the base of the Holocene succession. The base of the recovered peat interval has a low organic content (14%) and is better classified as a clayey peat, but it contains pieces of bark up to 7 cm long which were not sampled for the LOI measurement.

Unit 4 is a 0.5 m blue-gray loam which denotes the top of the Pleistocene strata. The Pleistocene-Holocene transition is commonly identified by a weakly developed paleosol (Törnqvist et al., 2004; Vetter et al., 2017) but this was not recovered in the core. Instead, the highly compacted blue-gray loam and the near-basal wood peat bracket this transition between 37.00 and 37.49 m depth.

4.3   *Grain-Size Analysis*

Grain-size analysis provides quantitative results to compare with qualitative sediment descriptions. Overall, the exact percentages of sand, silt, and clay of 58 samples were not predicted by the field descriptions but the sediment descriptions were generally good indicators of grain-size measurements (Fig. 9). While there is overlap between silty clay and silty clay loam textures, silty clay loam textures on average have higher silt contents than silty clays (Fig. 9). Additionally, grain-size results that plotted as silty clay loams were identified in the field as either silty clay loam or sandy loam. This may be due to sampling near laminations in intervals that contained both textures. Despite these

inconsistencies, grain size frequency curves of each description show that on average, each texture has a characteristic proportion of clay, silt, and sand (Fig. 10).

All discrepancies in the field descriptions were adjusted based on the grain-size measurements. For example, despite clay being described in the field, all clay samples had grain-size measurements that matched silty clays and have been corrected to reflect this. Furthermore, Pleistocene samples were originally described in the field as silty clay loam. This underestimated the sand content and overestimated clay and they have been corrected to loam in accordance with the grain-size measurements (Fig. 9). Unless explicitly noted as "field" descriptions (i.e., Table 2), all textures have been corrected.
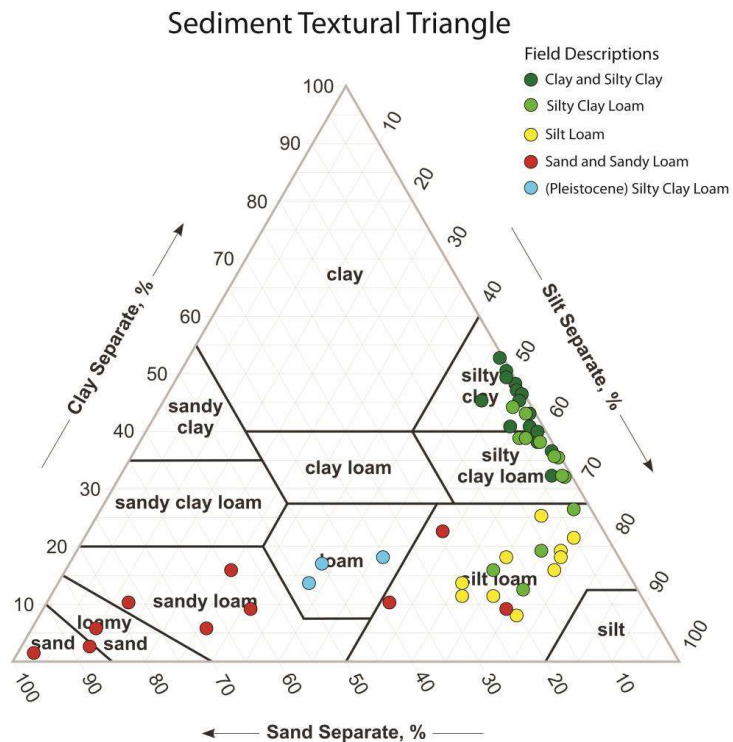
Figure 9 *Comparison of initial field descriptions with USDA classifications based on grain-size analysis.*

Overall, grain-size results confirm what is seen in the field descriptions (Fig. 11). Units 1 and 3 are heterogeneous with variable grain sizes; units 2 and 4 are homogenous with only minor variations in grain size. The overall trend shows that silt is dominant in unit 1, with peaks in clay near the modern marsh surface and sand near 6 and 10 m depth. The core then transitions into a consistent ratio of clay, silt, and sand throughout unit 2, which ends in unit 3. Unit 4 marks the top of the Pleistocene and is a loam texture, which has a grain-size composition that differs from all the Holocene samples.

Within unit 1, the sediment description for the top 5 m shows alternating silt loam and silty clay loam textures which are reflected by the D50 results, or the intercept for 50% of the cumulative frequency (Table 2; Fig. 11). Each of the three humic clay and peat beds are characterized by higher clay content (up to 60%) and lower D50 values (<13 μm), whereas the two sand beds show clay content <11% and D50 values >100 μm. The erosive contact at ~6.5 m should plot as a sharp drop in sand but due to sampling density and the low clastic content of peats, it is represented as a smoother transition.

Unit 2 shows a range in clay content from 30 to 48%. Each of the sampled intervals are silty clay or silty clay loam with very little sand (<6%). The only exception is the very top sample (12.1 m) which is a silt loam with 75% silt and a D50 of about 20 μm. It is coarser than all the other samples and is part of the transition from the sand bed at the bottom of unit 1 to the top of unit 2 which was only partially recovered during drilling.
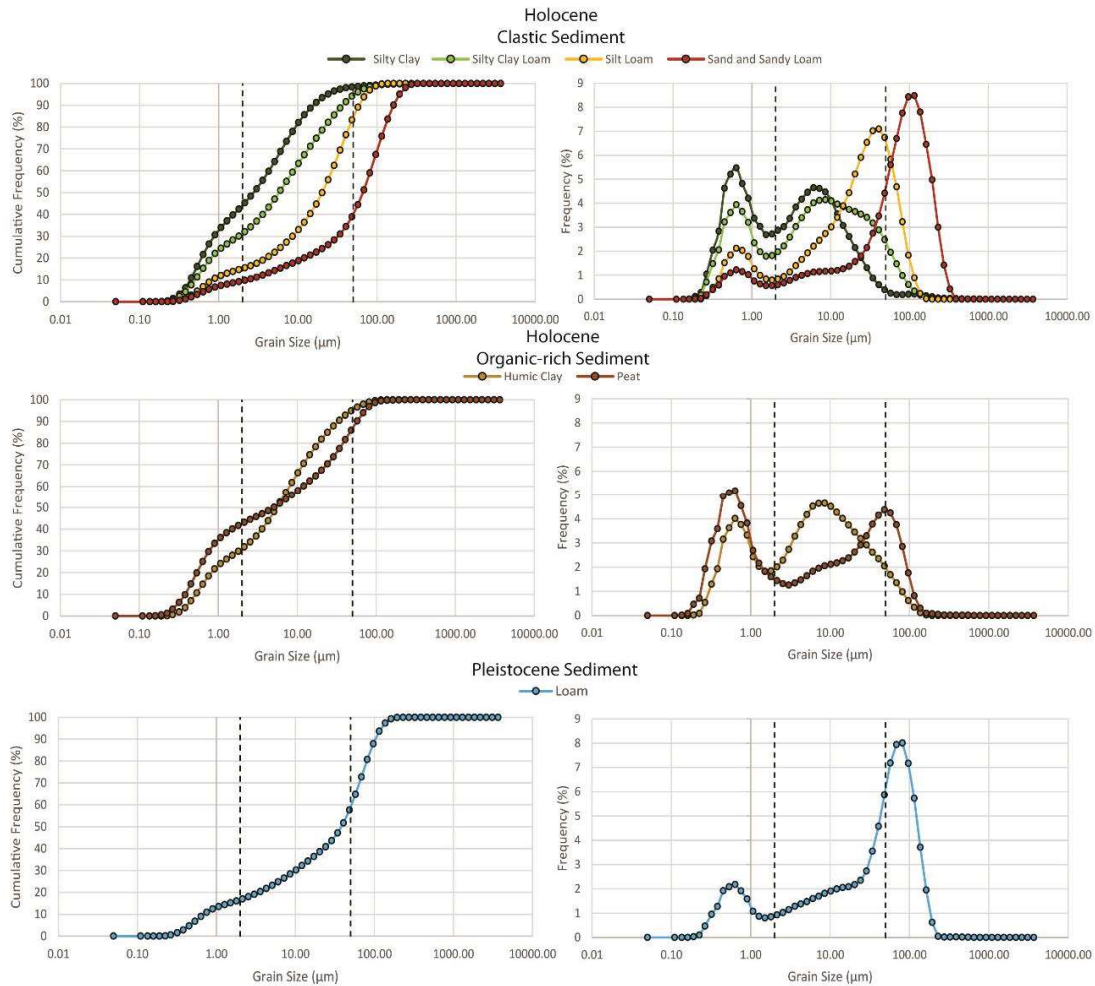
Figure 10*. Mean frequency curves and mean cumulative frequency curves for Holocene clastic and organic-rich (humic clay and peat) samples, and Pleistocene samples. Dashed lines represent the clay-silt (2 μm) and silt-sand (50 μm) transitions.*
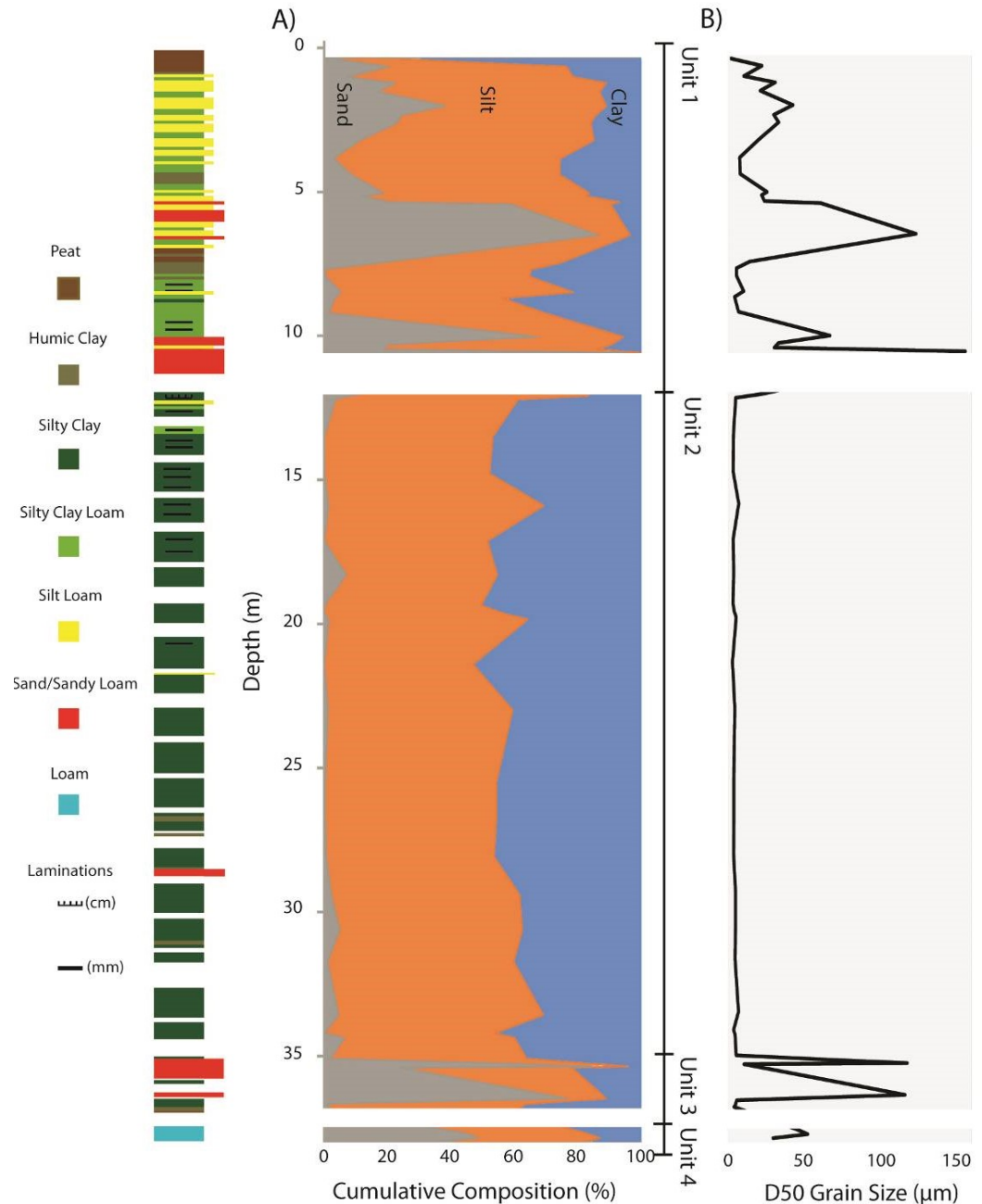
Figure 11 *Myrtle Grove I grain-size results, A) cumulative composition of clay, silt, and sand and B) D50 grain size plotted with the sedimentary log. White bars in plots represent gaps in data that did not allow interpolation due to facies transitions.*

Unit 3 consists of a meter-thick lag deposit that overlies a basal peat bed. The lag

deposit has a range of sand content with both clay and sand layers (Fig. 10). There is a

significant amount of shell hash in the lag deposit which was removed during sample preparation. The lowermost portion of the unit is a basal peat which has a 40% clay content. Unit 4 is a short interval of highly consolidated loam. Each of the three samples have similar grain size distributions and differ significantly from the Holocene samples.

Table 2 *Average grain size distribution and D10, D50, and D90 values by sediment texture class.*

Classification	D10 (µm)	D50 (µm)	D90 (µm)	Clay (%)	Silt (%)	Sand (%)	Number of Samples
Silty Clay	0.48	3.12	17.23	42.49	55.90	1.61	20
Silty Clay Loam	0.60	9.26	33.72	30.08	64.03	5.89	8
Silt Loam	1.32	23.19	62.44	14.69	68.58	16.73	8
Sand and Sandy Loam	12.61	78.50	150.24	9.22	26.67	61.07	10
Humic Clay	0.64	8.03	32.13	29.83	65.08	5.09	6
Peat	0.49	11.49	51.36	41.71	44.31	13.99	3
Loam	0.79	41.06	110.82	16.04	41.57	42.39	3

4.4   *Bulk Density Measurements*

The continuous bulk density measurements, which represent the raw bulk density of the saturated sediment plus the protective wax coating, reflect the variability seen in the physical description of the core (Fig. 8). This is evident by a strong qualitative correspondence between the sand-rich layers with the bulk density maxima and organic-rich layers with the bulk density minima. In order to convert raw bulk density to dry bulk density, several corrections were made. First, the paraffin wax, which has a bulk density of 0.9 g/cm^3, was removed from the continuous scanned bulk density to calculate a wet bulk density BD_{wet}:

$$BD_{wet} = ((BD_{raw} \times D_{container}) - (0.9 \times D_{wax}))/D_{sediment} \qquad (5)$$

where BD_{raw} is raw bulk density, $D_{container}$ is the diameter of the storage container (15.24 cm), $D_{sediment}$ is the diameter of the sediment core (12.7 cm), and D_{wax} is the difference of the container and sediment diameters (2.54 cm).

Next, the wet scan and the discrete, dry bulk densities were compared using regression analysis (Fig. 12A). Discrete measurements were taken from 2 cm thick samples and corresponding scanned bulk densities were averaged over a 4 cm interval which was centered on the sampled interval. This accounted for any uncertainty in depth. Next, the discrete, measured water content, w_c (Section 4.5), was removed from each corresponding interval in the wet bulk density scan, i.e., "dewatering" the scan using the equation:

$$BD_{dewatered} = BD_{wet} \times (1 - w_c/100) \qquad (6)$$

where $BD_{dewatered}$ is the dewatered bulk density. The dewatered bulk density scan and the discrete, dry bulk density have a strong correlation ($r^2 = 0.80$) and an almost 1:1 linear relationship (Fig. 12B). This strong relationship shows that discrete water content measurements are a reasonably accurate way to convert the wet bulk density scan to a dry bulk density scan but because w_c is not measured at a centimeter scale, the linear relationship between continuous, wet bulk density and discrete, dry bulk density is used (Fig. 12A) to convert the full wet bulk density scan to dry bulk density according to the equation:

$$BD_{dry} = 1.4297 \times BD_{wet} - 1.3594 \qquad (7)$$

a full, dry bulk density is calculated (Fig. 12C). Bulk density averages are reported in Table 3. The dry bulk density matches the discrete bulk density measurement ($r^2 = 0.62$) fairly well with comparable values in most of units 1 and 2. The biggest differences occur in the deeper sands where the linear relationship underestimates the dry bulk density (Fig. 12C).
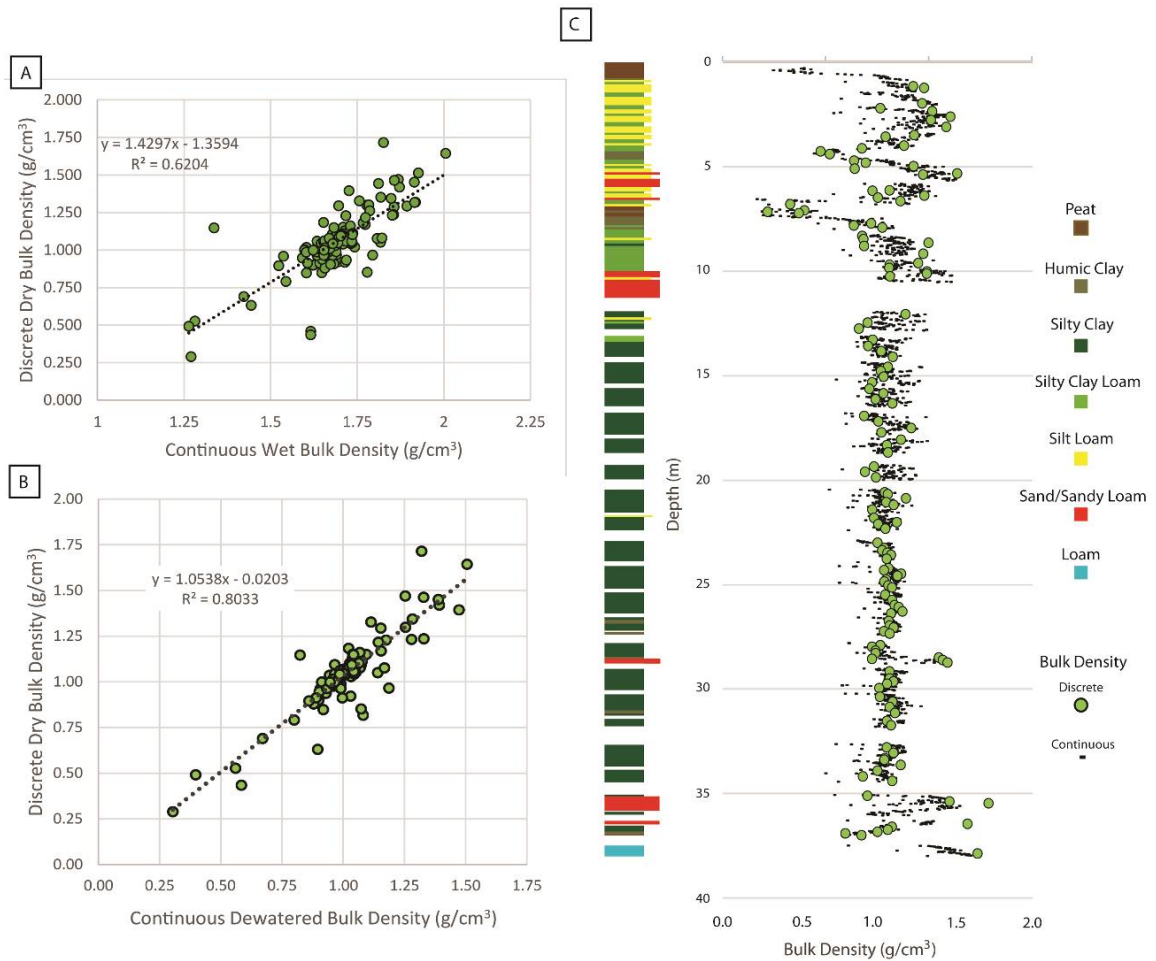
Figure 12 *Linear regression analysis of dry bulk density measured in the laboratory with A) wet bulk density scan data and B) dewatered bulk density scan data. The converted dry bulk density scan C) plotted alongside the discrete, dry bulk density data.*

4.5   *Water Content and Loss on Ignition*

Water content and LOI were measured for 138 samples chosen to represent the varying sediment textures and organic content within the core. In general, water content and LOI are highest in the organic-rich facies and lowest in the Pleistocene and sand-rich facies (Fig. 13, Table 3). In unit 1, the water content of clastic facies is generally lower but more variable than in units 2 and 3, whereas the LOI percentages are more variable than in units 2 and 3. In unit 4, water content and organic content are both low. Due to time constraints, these measurements were performed up to three months after dewaxing the core which introduces some uncertainty, despite samples being refrigerated at 2-3°C. Because atmospheric pressure is less than in situ pressures, water can be forced out of the void spaces between the sediment grains, decreasing water content. As a result, measured water contents should be treated as minimum values.

Table 3 *Organic matter and water content for each texture class from the Myrtle Grove I core.*

Sediment Texture	Mean Water Content (%)	Mean Organic Matter Content (%)	Dry Bulk Density (g/cm³)	Wet Bulk Density (g/cm³)	Number of Samples
Silty Clay	35.5 ± 2.6	5.6 ± 0.9	1.0 ± 0.1	1.4 ± 0.1	81
Humic Clay	46.2 ± 6.8	10.2 ± 2.5	0.8 ± 0.2	1.0 ± 0.2	6
Peat	66.2 ± 3.8	36.3 ± 7.9	0.4 ± 0.1	0.7 ± 0.1	4
Sand/Sandy Loam	22.2 ± 5.6	2.2 ± 0.6	1.4 ± 0.1	1.8 ± 0.2	12
Silty Clay Loam	33.3 ± 5.0	4.7 ± 1.4	1.1 ± 0.2	1.5 ± 0.1	20
Silt Loam	29.0 ± 6.1	3.1 ± 1.1	1.2 ± 0.2	1.7 ± 0.2	14
Loam	18.4	2.9	1.6	1.9	1
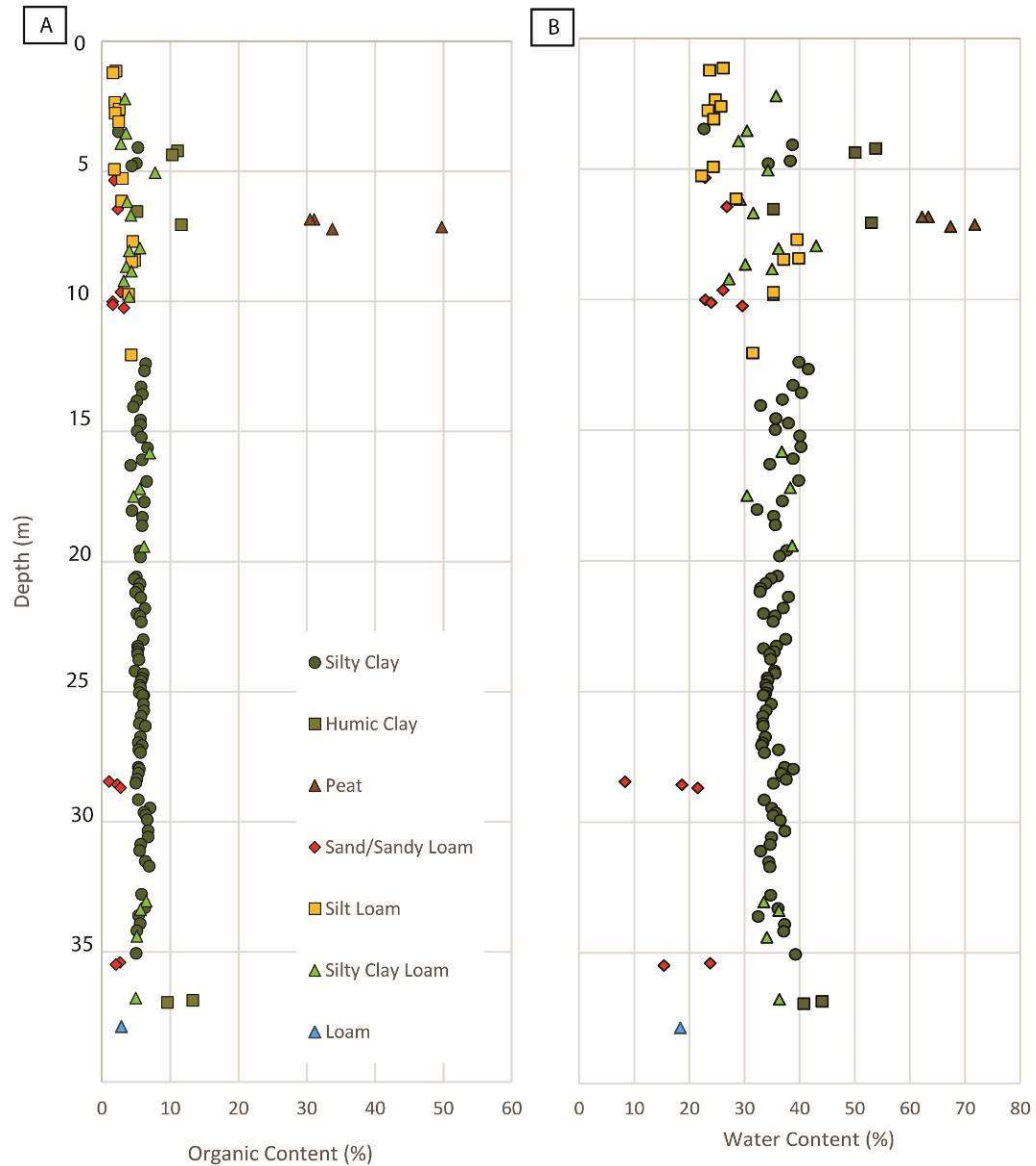
Figure 13 *Loss on ignition A) and water content B) plotted against depth and coded based on sediment textures and organic content.*

4.6   Geochronology

Each pair of radiocarbon samples from the intercalated peats (Myrtle Grove I-1 to I-3) produced highly consistent results from either seeds, charcoal, or both (Table 4). They agreed within 15 ^{14}C years and had analytical errors of $\pm$ 25 years. Radiocarbon ages for the near-basal peat (Myrtle Grove I-4) were a little further apart (9910 and 9780 ^{14}C yr

BP), despite similar error ranges to the intercalated peats. The weighted mean of the paired radiocarbon ages was converted to calendar ages (expressed in ka) for vertical displacement measurements (Section 5.3) and are reported in Table 10. The calibrated age ranges are reported with a 2σ error range.

In order to constrain the ages of the two sand beds in unit 1, four samples were dated using OSL (Table 5). Each of the sampled sands produced ages that agreed with the chronology from the radiocarbon ages (Fig. 8). The 1.8 m thick sand unit at 10-11.8 m depth was sampled three times to tightly constrain the age of deposition. This sand bed is laterally extensive over >2 km (Section 4.8) and formed between 3.0 and 3.7 ka.

Table 4 ^{14}C ages from the Myrtle Grove I core. The UTM zone is 16 N and coordinates are rounded to the nearest 5 m.

Sample Name	Lab Code	Northing (m) (NAD 83)	Easting (m) (NAD 83)	Z (m) (NAVD 88)	Depth below surface (m)	Material Dated	Sediment Texture	Age (^{14}C yr BP)
Myrtle Grove I-1a	UCIAMS-173664	3280135	214670	0.2	4.38-4.40	7 *Rhynchospora* sp. achenes	Humic Clay	1245 ± 25
Myrtle Grove I-1b	UCIAMS-173665	3280135	214670	0.2	4.38-4.40	1 charcoal fragment	Humic Clay	1260 ± 25
Myrtle Grove I-2a	UCIAMS-173666	3280135	214670	0.2	6.70-6.72	3 charcoal fragments	Humic Clay	2190 ± 25
Myrtle Grove I-2b	UCIAMS-173667	3280135	214670	0.2	6.70-6.72	5 charcoal fragments	Humic Clay	2200 ± 25
Myrtle Grove I-3a	UCIAMS-173668	3280135	214670	0.2	7.41-7.43	9 *Scirpus* spp. achenes	Peat	2955 ± 25
Myrtle Grove I-3b	UCIAMS-173669	3280135	214670	0.2	7.41-7.43	3 charcoal fragments	Peat	2945 ± 25
Myrtle Grove I-4a	UCIAMS-173670	3280135	214670	0.2	36.98-37.00	1 *Vitis* sp. seed	Clayey Peat	9910 ± 25
Myrtle Grove I-4b	UCIAMS-173671	3280135	214670	0.2	36.98-37.00	4 *Myrica* sp. infructescences	Clayey Peat	9780 ± 25

Table 5 *OSL ages from the Myrtle Grove I core. All ages are presented in ka relative to 2010. UTM Zone is 16 N and coordinates are rounded to 5 m.*

Sample Name	Lab Code	Northing (m) (NAD 83)	Easting (m) (NAD 83)	Z (m) (NAVD 88)	Depth below surface (m)	Sediment Texture	Age (ka)
Myrtle Grove I-5	NCL-1217135	3280135	214670	0.2	5.55-5.65	Sand	1.17 ± 0.12
Myrtle Grove I-6	NCL-1217138	3280135	214670	0.2	10.01-10.06	Sand	3.07 ± 0.35
Myrtle Grove I-7	NCL-1217136	3280135	214670	0.2	10.40-10.50	Sand	3.36 ± 0.28
Myrtle Grove I-8	NCL-1217137	3280135	214670	0.2	10.90-11.00	Sand	3.71 ± 0.28

4.7   *Paleoenvironmental Analysis*

In order to reconstruct the local paleoenvironment of the organic-rich facies, $\delta^{13}C$ analysis was carried out on bulk material associated with the ^{14}C samples. Within each depth interval, duplicate or triplicate samples were consistent with each other and showed minimal deviations in $\delta^{13}C$ values and inferred paleosalinities (Table 6). Sample Myrtle Grove I-1 $\delta^{13}C$ results indicate it formed in a freshwater environment which is consistent with macrofossil analysis (Table 6) (Chmura et al., 1987). Because the sample is a freshwater humic clay, the elevation during formation of the sample is unknown. Sample Myrtle Grove I-2 formed in a brackish or saline environment which was between mean tide level (MTL) and highest astronomical tide (HAT). Because HAT is not well known for the region, mean higher high water (MHHW) is used instead, which provides a range of ~30 cm (González and Törnqvist, 2009; Hijma et al., 2015). Myrtle Grove I-3 results indicate a freshwater environment near the minimum salinity that *Scirpus* generally grows in (Chmura et al., 1995) (Table 6). These results indicate that the base of this peat bed formed above sea level, possibly at or above MHHW, whereas the top of this peat bed formed within the intertidal zone. The deepest sample, Myrtle Grove I-4, formed in a wetland

environment that, in terms of salinity, was between brackish and fresh, or "intermediate". Intermediate environments have diverse populations of both fresh and brackish marsh plant species (Louisiana Natural Hertiage Program and Louisiana Department of Wildlife and Fisheries, 2009) which may be the reason why macrofossils suggest a lower salinity.

Table 6 *δ¹³C bulk sample results from the Myrtle Grove I core.*

Sample Name	Depth below surface (m)	Sediment Texture	δ^{13}C PDB (per mil)	Macrofossils	Environment
Myrtle Grove I-1	4.38-4.40	Humic Clay	-26.11, -26.19	*Rhynchospora* sp.	Fresh
Myrtle Grove I-2	6.70-6.72	Humic Clay	-17.37, -17.64	N/A	Brackish or Saline
Myrtle Grove I-3	7.41-7.43	Peat	-27.27, -27.77, -27.91	*Scirpus* spp.	Fresh
Myrtle Grove I-4	36.98-37.00	Clayey Peat	-23.19, -24.01, -24.53	*Myrica* sp. and *Vitis* sp.	Intermediate

4.8   Regional Stratigraphy

The Myrtle Grove cross section consists of nine boreholes that were drilled to depths of ~12 m to examine the lateral extent of deposits found in the upper portion of the Myrtle Grove I core. The cross section is a little over 2 km long and is oriented perpendicular to the modern Mississippi River (Fig. 14). The present-day land surface at the northeastern side is a poldered field and the southwestern side is located in the modern marsh. Four boreholes were taken in the field and five, including the Myrtle Grove I borehole, in the marsh. Boreholes are spaced roughly 200 m apart, but borehole placement was ultimately determined by where in the marsh it was easiest to stand. In reference to the previously defined units 1-4, the cross section contains all of unit 1 and a few meters of unit 2.

Figure 14 *Location map of the cross section with the nine boreholes.*

The Myrtle Grove I core (ID # 601692-001) is used in the cross section; an additional hand core was drilled at the same location in order to fill in gaps due to incomplete recovery in the Fugro core. This hand core (ID # 601792-001) is supplementary to the Fugro core and confirms the depths of the peat and sand beds at the Superstation site.

The top of the cross section contains a 1.2 ± 0.2 m thick peat bed that represents the modern marsh. It is laterally extensive across most of the cross section but does not extend into the poldered field (Fig. 15). Underlying the surface peat is 3.8 ± 1.0 m of variable sediment textures that include peat, humic clay, silty clay loam, silt loam, and sandy loam. The different textures are not laterally extensive across the entire 2+ km but a few layers, such as the sand and sandy loam at a depth of ~3-4 m extend over 1 km. The base of these sand and sandy loam deposits form an erosive contact with the underlying, 1.1 ± 0.1 meter thick intercalated peat (Fig. 15). This peat is laterally extensive, with some variations in elevation and shells are found on top of it in several boreholes (Appendix B,

Fig. B.1). The erosive contact found at the top of the intercalated peat is noted in several other boreholes.

Below the intercalated peat is 1.6 ± 0.4 m of overbank sediment. The deposits consist of silty clay loam and silt loam and are laterally extensive. These deposits overlie a major sand body that varies in thickness. The sand is laterally extensive, thins towards the distal end of the cross section, and is composed of fine and medium sands. Three OSL ages from this sand body indicate that deposition occurred between 3.0 and 3.7 ka. The deeper sands overly silty clay loam and silt loam which contain silt laminations that thin with depth. Some shells were found in these deposits but not across the entire region. As previously outlined (Section 4.2), these deposits transition into a 20+ m thick deposit of silty clays which are a part of unit 2.

Most sediment bodies are laterally extensive throughout the cross section but the elevation of facies boundaries can differ between boreholes. This is best illustrated when comparing the elevation of the intercalated peat in the Myrtle Grove I core to the rest of the cross section (Fig. 15). The base of the peat is at -7.3 m at the Superstation site and between -4.7 and -5.5 m in the other boreholes. The implications are discussed in Section 5.3.
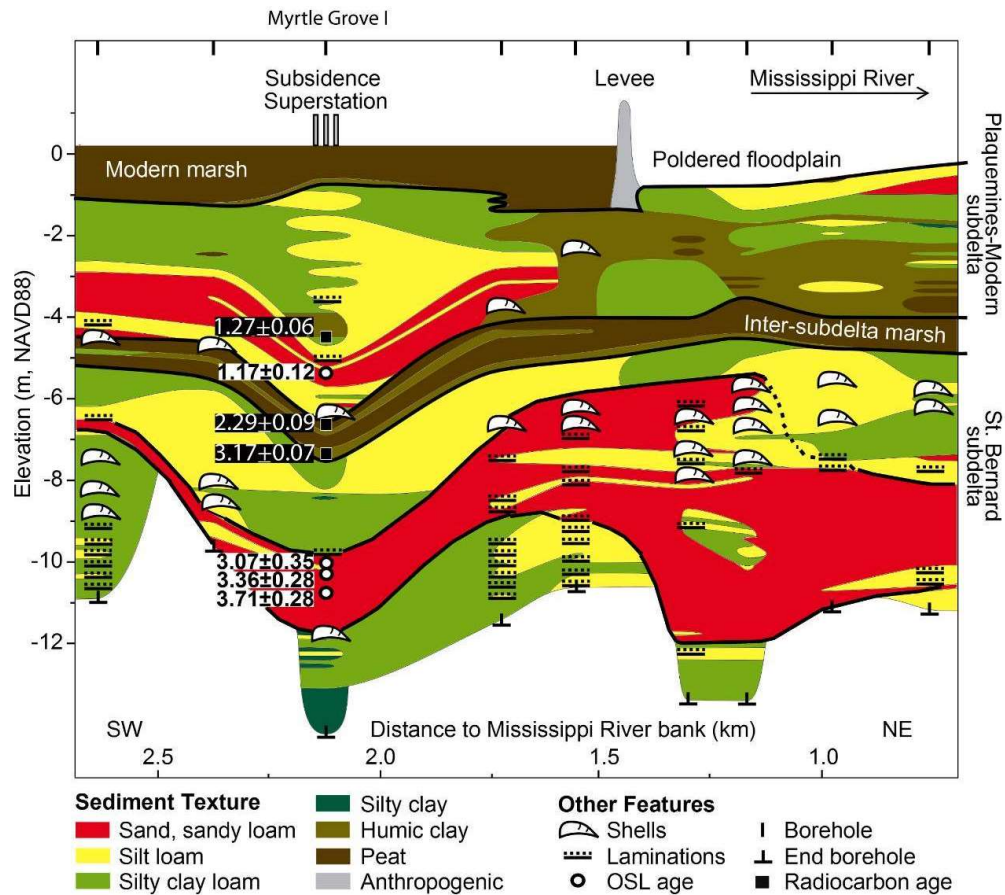
Figure 15 *Hand-cored cross section showing the lateral extent of deposits found in the Myrtle Grove I core.*

4.9   Consolidation Testing

Eight 1-D consolidation tests were performed on samples from the Myrtle Grove I core (Section 5.2, Fig. 18). Each sample was given the prefix "CS" for consolidation sample and a number that corresponded to the depth of recovery rounded to the nearest meter (Table 7). Sample CS-3 (depth of ~3 m) is not included in further analysis because of a dial gauge error during testing, but the data are available in Appendix C (Fig C.1). Despite careful handling, all the remaining seven samples are described as C and D sample designation based on Terzaghi et al. (1996). This means that the sample qualities are highly disturbed which is likely due to extrusion, drilling, and handling procedures. The

methodology to determine sample quality is outlined in Lunne et al. (1997) but is essentially determined by calculating the change in void ratios from consolidation testing results and comparing it to the expected void ratio based on the overlying sediment (Lunne et al., 1997). Disturbance reduces the sharp break in behavior at the preconsolidation stress and can affect the compression index (C_c) (Terzaghi et al., 1996, Lunne et al., 1997).

Measured parameters include the C_c that relates to the magnitude of primary consolidation for normally consolidated soils, i.e., larger values indicate more settlement. Typical values in the MRD generally range from 0.05 for sands, to 0.70 for prodelta clays, to >0.93 for organic-rich deposits (Montgomery, 1974; Kuecher, 1994). The permeability coefficient (C_k), which can be empirically estimated using $C_k = 0.5*e_o$, indicate that for higher values, hydraulic conductivity decreases more rapidly with increased effective vertical stress (σ'_v). Initial void ratio (e_o) was determined by measuring the moisture content (w_c) and assuming a specific gravity of 2.65 for a saturated sample (water table is at the ground surface). Atterberg limits (plastic limit (PL), liquid limit (LL), and plasticity index (PI)) were determined following the ASTM D4318-17 test method (ASTM International, 2017b) and are used to classify soil types, which are a function of fine-grain (<74 µm) content, clay minerology, and depositional environment (Das, 1990; Terzaghi et al., 1996). Lastly, effective vertical stress (σ'_v) is calculated from the depth and bulk density measurements, and maximum stress (σ'_n) from the corresponding log stress-e plots using the Sowers (1970) and Casagrande (1936) methods (Fig. 16).

In this section, an additional sediment classification system (the Unified Soil Classification System, or USC) will be denoted along with USDA classifications (Table 7 and 8). USC classifications are the standard format for geotechnical measurements and are

determined using grain size, organic content, LL, and PI following ASTM D 2487 (ASTM

International, 2017c).

Table 7 *Geotechnical properties and Atterberg Limits for the consolidation samples from the Myrtle Grove I core. Effective stress and maximum stress are calculated from the log stress-*e *plots and bulk density measurements, respectively, and over-consolidation ratio is equal to the maximum stress divided by the effective stress. Water content is calculated following standard geology methods.*

Sample ID	USCS Soil Classification	Average Depth (m)	C_C	w_c (%)	e_o	σ'_v (kPa)	σ'_n (kPa)	OCR	C_k	LL (%)	PI (%)
CS-2	CL	1.85	0.23	23.08	0.80	14.71	22.95	1.56	0.26	25.9	10.7
CS-8	CL	7.60	0.60	30.24	1.15	45.66	52.50	1.15	0.40	42.6	21.2
CS-10	CL	10.31	0.55	28.12	1.04	69.30	63.84	0.92	0.58	43.7	19.7
CS-12	CL	12.00	0.41	27.07	0.98	78.54	50.38	0.64	0.51	39.3	19.0
CS-20	CL	19.54	0.61	27.72	1.02	116.00	111.27	0.96	0.56	47.4	22.8
CS-34	CL	34.10	0.52	26.23	0.94	179.14	304.12	1.70	0.29	46.5	23.2
CS-38	CL	37.62	0.20	17.33	0.56	198.46	159.25	0.80	0.10	38.7	20.0

All consolidation test samples were identified as inorganic clays with low to medium plasticity, or CL (Table 7). Despite the similar classifications, there were considerable differences between some of the samples. The results show that five samples (CS-8 to CS-34) behave in a manner consistent with each other (Fig. 16) because of similar Atterberg limits, geotechnical values (C_c, e_o, and C_k), and water content (Table 7). This is likely due to similar sediment mineralogy and grain orientation, but these have not been looked at in detail in this study. Sample CS-2 is a CL, like all the other samples, and per USDA classifications is a coarse silt loam which indicates it has a higher silt and sand content than samples CS-8 to CS-34 (Table 7). Even though CS-2 is the shallowest sample (1.85 m), it is the least compressible of all the Holocene samples (CS-2 to CS-34). CS-38 also exhibits a low compressibility even though it is a CL, but this could be due to a relatively higher sand content (USDA loam) (Table 8) and because it is a Pleistocene sample. This difference in stress history, age, and sediment properties results in the lowest

C_c, e_o, w, and C_k values (Table 7). All samples, except for CS-2, have liquid limits (LL) of

~40% and plasticity indexes (PI) of ~20%. CS-2 has a LL of 26% and a PI of 10.7% which

is likely due, along with its other properties, to the low clay (11.0%) and high sand (38.4%)

content. It is important to note that the USCS and USDA systems are not directly relatable

and extrapolations of geotechnical values based on USDA textures are not standard

practice.

Table 8 USDA and USCS soil characteristics and classifications for consolidation
samples.

Sample ID	Average Depth (m)	LL (%)	PI (%)	USCS Soil Classification	Clay (%)	Silt (%)	Sand (%)	USDA Sediment Texture
CS-2	1.85	25.9	10.7	CL	11.0	50.7	38.4	Silt loam
CS-8	7.60	42.6	21.2	CL	34.7	65.2	0.1	Silty clay loam
CS-10	10.31	43.7	19.7	CL	14.2	67.2	19.6	Silt loam
CS-12	12.00	39.3	19.0	CL	16.9	74.9	8.2	Silt loam
CS-20	19.54	47.4	22.8	CL	42.9	57.0	0.1	Silty clay
CS-34	34.10	46.5	23.2	CL	46.3	63.6	0.1	Silty clay
CS-38	37.62	38.7	20.0	CL	17.4	38.0	44.6	Loam

Preconsolidation stress, (σ'_p), and the *in situ* effective vertical stress (σ'_{vo}) were

estimated to calculate overconsolidation ratios (OCR) (Table 7). If a sample is

overconsolidated (OCR > 1), it is less compressible than an identical, normally

consolidated sample (OCR ~1) (Terzaghi et al., 1996). The OCR of CS-2 is 1.56 so it is

slightly overconsolidated because of desiccation or erosion of overlying sediment that was

replaced with the less dense modern marsh surface (Fig. 8). The OCR of CS-34 is

approximately 1.7, which is unlike the other normally consolidated prodelta samples (CS-

12 and 24). This difference is demonstrated in Fig. 16 by the log σ'_v – e relationships,

where CS-34 overlies CS-12 and CS-24. In other words, CS-34 shows a stiffer behavior than other prodelta deposits, whereas the PI, LL, and particle size gradation indicate similar physical index properties.
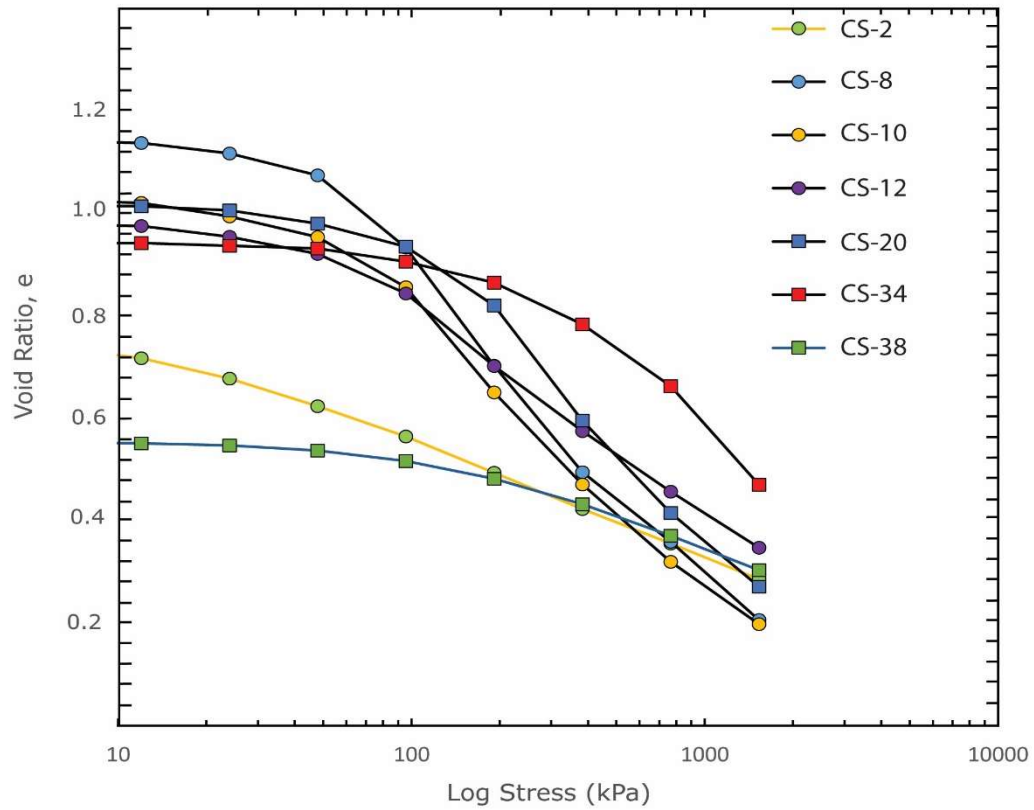
Figure 16 *Log stress-*e *plots for seven samples from the Myrtle Grove I core.*

5.   DISCUSSION

5.1   Lithogenetic Units

Sediment and geotechnical properties describe a wide range of attributes for both the Myrtle Grove I core and the region covered in the cross section. Using grain size, organic content, and stratigraphic relationships, different lithogenetic units (often composed of multiple facies) and smaller features within them can be identified (Table 9).

Overbank deposits form when the river floods, with the coarsest sediment being deposited close to the banks and finer grains more distally. These deposits are found within the top 10 m of the core (unit 1) and are relatively fine-grained, consisting of alternating silty clay loam and silt loam textures with low organic content (<15%). Overbank deposits can also be broken into lithogenetic subunits that include natural-levee, crevasse-splay, and flood-basin deposits.

Mouth-bar deposits form very rapidly as the delta progrades seaward with the top of the deposit, or the mouth-bar/overbank (MO) transition, corresponding to low mean tide, ~20 cm below sea level in this region (Wellner et al., 2005; González and Tornqvist, 2009). Mouth-bar sands are thick, coarse-grained sediment bodies that are laterally extensive across the region. Generally, they are thicker in the proximal reaches and pinch out away from the river. In the Myrtle Grove cross section, the sand between a depth of 7 and 12 m is interpreted as a mouth-bar deposit following the above criteria and interpretations of the overbank and delta-front (discussed below) deposits (Fig. 17).

Bay-floor and delta-front deposits are lower energy deposits than mouth-bar sands and often underlie them. Delta-front deposits are characterized by fine-grained silty clay loam with sand or silt laminations, whereas bay-floor deposits are generally a

homogeneous silty clay loam texture with shells. In the Myrtle Grove I cross section both delta-front and bay-floor deposits are found below the mouth bar (Fig. 17). Below 12 m in the Myrtle Grove I core, delta-front deposits are identified by the silt and sand laminations (Appendix B, Fig. B.3) which decrease in frequency with depth to ~17 m. Below this (~17-35 m), the silty clay muds are more homogenous and are interpreted as prodelta deposits (Appendix B, Fig. B.4).

Marsh deposits are characterized by intercalated peats which include peat, clayey peat, and humic clay. These deposits represent periods of lower clastic sedimentation rates which allowed for significant amounts of organic accumulation. In the cross section, peat and humic clay beds between a depth of ~4.5 and ~7 m are identified as marsh deposits (Fig. 17).

Table 9 *Characterization of clastic lithogenetic units that were identified by sediment texture, sedimentary structures, and other features found in the Myrtle Grove I core.*

Lithogenetic Unit	**Dominant sediment texture**	**Sedimentary structures and other features**
Overbank deposits	Silty clay loam, silt loam, silty clay, clay, humic clay	Highly variable, may contain wood and herbaceous material
Mouth-bar deposits	Sand (very fine to medium)	Homogenous
Delta-front deposits	Clay, silty clay, silty clay loam, silt loam	cm-scale laminations, reworked organics, coarsening-upward
Bay-floor deposits	Clay, silty clay, silty clay loam	*Rangia cuneata*, storm-reworked layers of shell hash
Prodelta deposits	Clay, silty clay	Homogeneous

The dating of the intercalated peat found at a depth of ~4.5 to ~7 m in the cross section shows that sedimentation rates were very low between 2.3 and 3.2 ka and most of

the river's sediment load was being deposited elsewhere in the delta during this time. This indicates that above and below the intercalated peat there are two different subdeltas. OSL dating of the mouth-bar sands (3.71-3.07 ka) indicates that the lower subdelta is the St. Bernard, based on a previously established chronology (Törnqvist et al., 1996). The OSL and radiocarbon ages from the shallower subdelta indicates that it is the Plaquemines-Modern (Fig. 17). The sandy deposit in the Plaquemines-Modern subdelta is interpreted as a crevasse-splay deposit because it is isolated from the Mississippi River, laterally extensive over only 1 km in the cross section, and has a coarser grain size than the rest of the overbank deposits (Fig. 17).
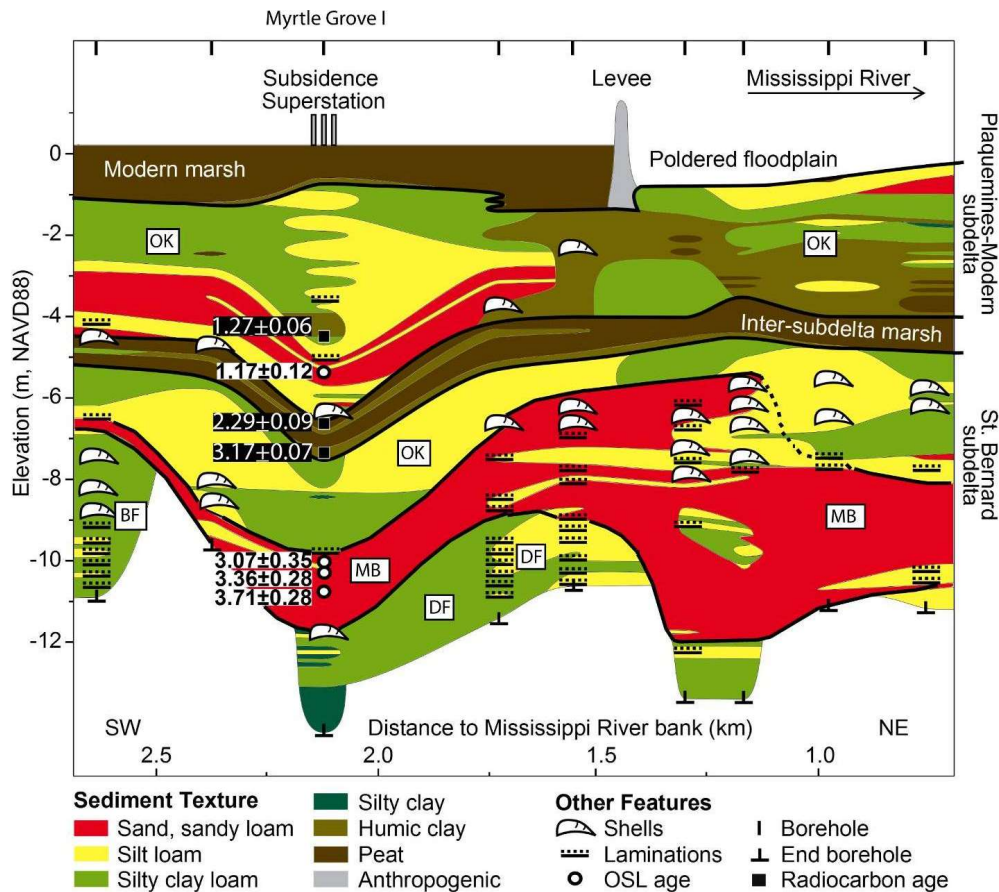
Figure 17 *Hand-cored cross section showing the lateral extent of upper Holocene strata found in the Myrtle Grove I core. Lithogenetic units are marked by abbreviations for overbank (OK), mouth-bar (MB), bay-mud (BF), and delta-front (DF).*

5.2   *Landscape Evolution*

At the end of the Pleistocene, the landscape around the Superstation was a subaerial alluvial terrace. This corresponds to a depth of 37.5-38.0 m in the core; further mention of core depths will be denoted in parentheses. As sea level rose through the early Holocene, a basal peat started to form on top of the Pleistocene surface. Around 11.3 ka, relative sea level was still below -36.8 m (NAVD 88) which is indicated by the low salinity and macrofossils found in the near-basal peat. Furthermore, trees inhabited the site, as indicated by bark found in the peat (Appendix B, Fig. B.2), and the site was an intermediate environment with both fresh and brackish marsh species (Louisiana Natural Heritage Program and Louisiana Department of Wildlife and Fisheries, 2009).

The near-basal peat found close to the Pleistocene-Holocene transition in the Myrtle Grove I core offers an approximate upper limiting sea-level data point (Fig. 18), indicating that sea-level was below –37 m around 11.3 ka years ago. There is some uncertainty in the elevation of this limiting data point due to compaction of the underlying organic peat. The extent of the underlying organic unit is poorly constrained because the Pleistocene-Holocene transition was not recovered but the maximum amount of compacted peat below sample Myrtle Grove I-4 is 0.5 m in thickness.

As sea level continued to rise in the early Holocene, a silty clay mud was deposited (Appendix B, Fig. B.2) (36.5-36.8 m), some of which was eroded as the shoreline transgressed past the site. This created a ravinement surface and a lag deposit which is interpreted from the over 1 m of reworked clay, sand, and shells (35.1-36.5 m) (cf. Nummedal and Swift, 1987). The site remained subaqueous throughout the early and middle Holocene as the Mississippi River deposited clays and silts which built up a ~23 m

thick deposit. There are no age constraints on the timing of deposition but ~17-35 m depth is interpreted as a prodelta deposit because it is a homogenous silty clay with few laminations. The proximity of the site to the Mississippi River in the early Holocene is unknown but prodelta deposits can accumulate rapidly depending on the proximity of the mouth bar and the water depth. Above 17 m, mm and cm-scale laminations are present and decrease in frequency with depth. These are interpreted as delta-front deposits and imply that the river mouth was closer to the site. In order to better constrain the timing of deposition, a dating technique such as ramped pyrolysis ^{14}C dating could be used in the delta-front and prodelta deposits.

By 5.7 ka, rates of sea level rise had slowed enough for the Mississippi River to start building the Teche subdelta west of the Superstation site and between 3.8 and 4.0 ka, the Mississippi River began to also build the St. Bernard subdelta more proximally and east of the area (Törnqvist et al., 1996; Hijma et al., 2017). As the St. Bernard system captured more of the Mississippi River discharge, which increased sediment supply in the study area, the delta prograded past the Superstation. At around 3.4 ka (the weighted mean age of the three mouth bar OSL ages) the mouth bar had been fully deposited (10.0 – 11.9 m) and the site was approximately at low mean tide, which is -0.2 $\pm$ 0.1 m below mean sea level across the delta (González and Törnqvist, 2009).

The site soon became subaerial due to continued St. Bernard overbank sedimentation that built up several meters of overbank deposits (7.5-10.0 m). When sedimentation rates decreased around 3.1 ka, a fresh water marsh began to form and by 2.2 ka, the marsh had become brackish, indicating shoreline transgression towards the site (6.7-7.5 m). After 2.2 ka, the Mississippi River abandoned the St. Bernard lobe

(Hijma et al., 2017), the marsh was drowned, and the landscape transformed into a bay which is evident by the shells on top of the inter-subdelta marsh. It is unclear how long the bay persisted but as early as 1.4 ka, the Mississippi River began to form the Plaquemines-Modern subdelta (Hijma et al., 2017) and by 1.2 ka, a crevasse splay had eroded most of the bay deposits at the site.

The landscape quickly aggraded as indicated by the similar ages of the two shallowest dated samples (1.27 ± 0.06 and 1.17 ± 0.12 ka) which are only one meter apart. Overbank sedimentation continued at the site (0.9-5.3 m) until the levees were artificially raised, cutting off the majority of the sediment supply to the modern marsh (0.0-0.9 m). As previously outlined, sedimentation was artificially stymied as early as 1888 by landowners and more fully in 1928 with the creation of the federal MR&T levees (Plaquemines Parish, 2014).
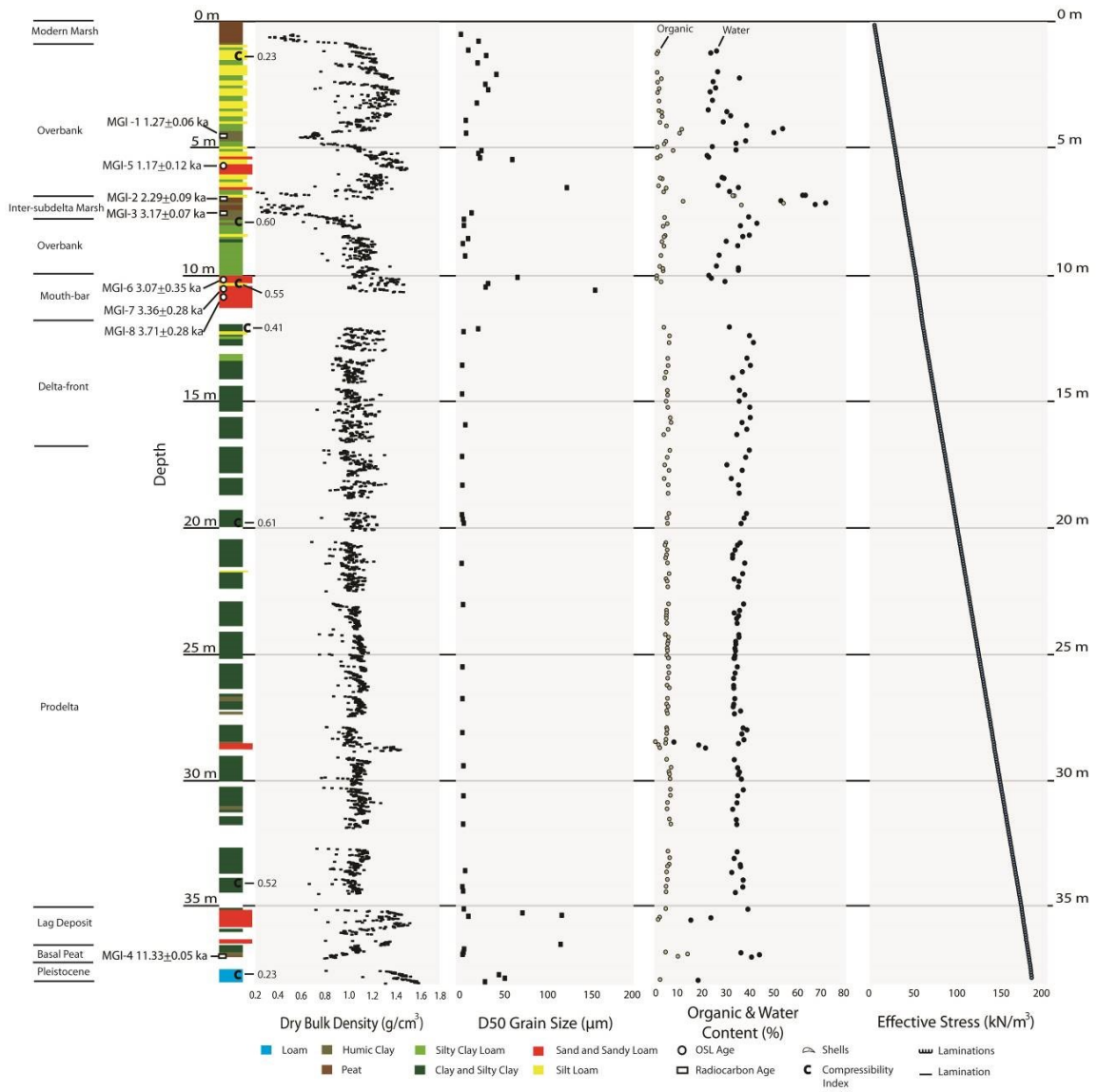
Figure 18 *Compilation of sediment and geotechnical measurements and interpretations of the Myrtle Grove I core. Effective stress is measured on a decimeter scale using bulk density averages. Radiocarbon ages are calibrated and all ages are relative to 2010 CE.*

5.3   *Local Subsidence Rates*

Using ^{14}C dated peat and OSL dated mouth-bar sands, it is possible to measure rates of vertical displacement within the Myrtle Grove I core. In order to account for deep subsidence processes, such as glacial and sediment isostatic adjustment (GIA and SIA,

respectively), the dated samples are compared to a basal-peat derived relative sea-level record from elsewhere in the MRD, as synthesized by Yu et al. (2012).

Basal peats approximately record relative-sea level rise. The underlying strata, in this case the Pleistocene, exhibits negligible compaction over the Holocene so by comparing the present data set to basal peat records in the MRD, GIA is removed because it affects both data sets equally. This means that shallow (compaction) and local, deep processes (faulting, fluid extraction) are captured in the vertical displacement calculation. At the Bird's Foot, SIA is about 0.5 mm/yr (Wolstencroft et al., 2014) so at the Superstation it should be much less and is not considered in further detail.

The basal peat record found on top of the Pleistocene alluvial terrace was collected from sites all across the MRD and has been used to construct a relative sea-level curve for most of the Holocene. Yu et al. (2012) created a standardized database that provides a highly robust and precise relative sea-level record that allows this study to remove the effects of GIA from vertical displacement measurements. The relative sea-level curve is used to calculate the original elevation for four dated samples based on their age. This elevation has a range that carries several uncertainties such as non-vertical drilling, sampling, surveying, and formation elevation range. By identifying the wetland environment based on macrofossils and stable carbon isotope results, a relationship can be made to sea level. Brackish samples, such as Myrtle Grove I-2, form between mean higher high water (MHHW) and mean tide level (MTL), which in the MRD is within a +0.3 m range of sea level (Törnqvist et al., 2004). Samples identified as freshwater (Myrtle Grove I-1 and I-3) only have minimum formation elevations of MTL so all measurements are minimum values. OSL samples from the mouth-bar sands form slightly below sea level.

The mouth bar/overbank transition, or M-O transition, occurs at the top of the sand and forms at low mean tide (Wellner et al., 2005). Low mean tide is estimated by González and Törnqvist (2009) to be -0.2 ± 0.1 m below mean sea level. Because mouth-bar sands form rapidly and within the resolution of OSL dating (Chamberlain, 2017), formation age is determined by the weighted mean of the three OSL ages.

In order to calculate vertical displacement, each sample is matched to the RSL curve based on age and total vertical displacement is calculated following the equation:

$$Vertical\ Displacement = (E_r - E_f) \qquad\qquad (8)$$

where E_f is original elevation and E_r is the recovery elevation midpoint. Displacement rate is then calculated by dividing vertical displacement by the time elapsed since formation (Fig. 19, Table 10)(Haslett et al., 1998; Törnqvist et al., 2008). For samples Myrtle Grove 1 and 3, vertical motion and rates are minima because formation elevation is only constrained by MTL and they do not have upper bounds.
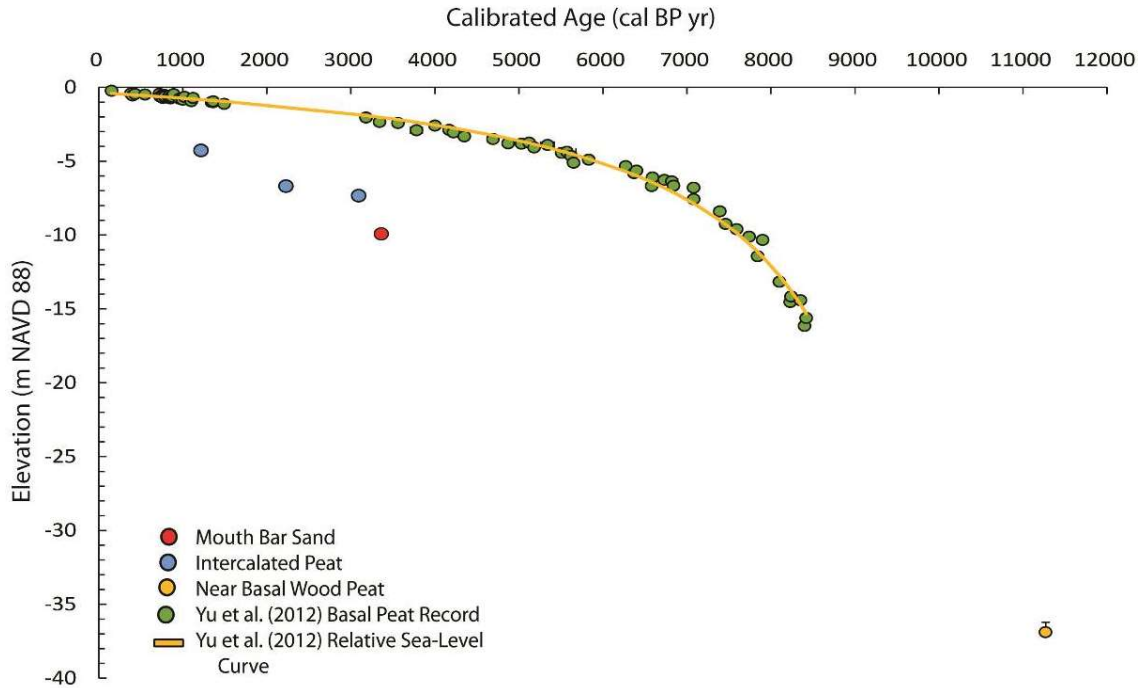
Figure 19 *Holocene relative sea-level curve for the MRD obtained from basal peat data (Yu et al., 2012). The yellow line is fit to the green points following the equation y = (a+cx)/(1+bx) where a = -0.22972607, b=-9.604e-05, c=-0.00031812, r^2: 0.99, and Fit Standard Error: 0.36 m.*

The elevation of samples within the core is well known but there is some uncertainty concerning variations in the elevation of facies transitions across the region (Fig. 17). The additional boreholes drilled for the Myrtle Grove cross section show that the depth of the inter-subdelta marsh and the St. Bernard mouth bar are shallower across the region than in the Myrtle Grove I core. The depths from the Myrtle Grove I core are not erroneous and were confirmed with the Myrtle Grove hand core (Section 4.8). These elevation differences are likely due to differential loading which assumes that these transitions have similar ages throughout the region. This assumption is used for the vertical displacement calculations and this variability must be taken into account (Table 10).

Table 10 *Vertical displacement and mean displacement rates for samples from the Myrtle Grove I core. Elevation ranges reflect possible depth ranges across the region. Formation elevation is calculated following the equation $y = (a+cx)/(1+bx)$ where $a = -0.22972607$, $b=-9.6604e{-}05$, $c=-0.00031812$ (Yu* et al.*, 2012). The Myrtle Grove I-6/7/8 elevation is taken from the top of the mouth bar and the weighted mean is taken from all three OSL ages.*

Sample Name	Facies Contact Elevation Range (m)	Formation Elevation (m)	Vertical Displacement (m)	Weighted Mean Age (ka)	Mean Displacement Rate (mm/yr)
Myrtle Grove I-1	-4.17 to -4.19	-1.06 +	3.12 +	1.27 ± 0.06	2.46 +
Myrtle Grove I-2	-4.14 to -6.50	-1.05 ± 0.51	2.58 to 5.96	2.29 ± 0.09	1.12 to 2.60
Myrtle Grove I-3	-4.80 to -7.21	-2.09 +	2.71 +	3.17 ± 0.07	0.85 +
Myrtle Grove I-6/7/8	-6.64 to -9.80	-2.12 ± 0.46	4.06 to 8.04	3.43 ± 0.18	1.18 to 2.34

At the Superstation site, sediment compaction, faulting, and fluid extraction are all potential contributors to the measured vertical displacement. Even though they are deep subsurface processes, faulting and fluid extraction are not accounted for through a comparison with a basal peat record because of their localized effects. Fluid extraction records have been collected by the Louisiana Department of Natural Resources since 1977 and are readily available through the online database SONRIS (www.sonris.com). Oil field traces were drawn around the outermost wells in each of the fields and the closest field, Lafitte, is about 4 km from the Superstation (Fig. 20). Subsidence due to decreases in pore pressure from fluid withdrawal is known to occur in the MRD (Kolker et al., 2011) and subsidence rates can even increase after extraction ceases (Chang et al., 2014). While modeling of the Lafitte reservoir would be required to calculate subsidence due to extraction, analogs can be found in other fields. At the Cerro Prieto field in Baja California, rates of subsidence are observed to be highest near the center of the reservoir and rapidly decrease away from the reservoir (Carnec and Fabriol, 1999). If this is assumed to apply

for the effects of fluid extraction at the Lafitte Field, then subsidence due to fluid extraction would be minimal at the Superstation. Groundwater withdrawal is also not a factor because the only wells reported in the SONRIS database within 3 km of the Superstation are monitoring wells (< 15 m deep) which extract negligible amounts of groundwater.
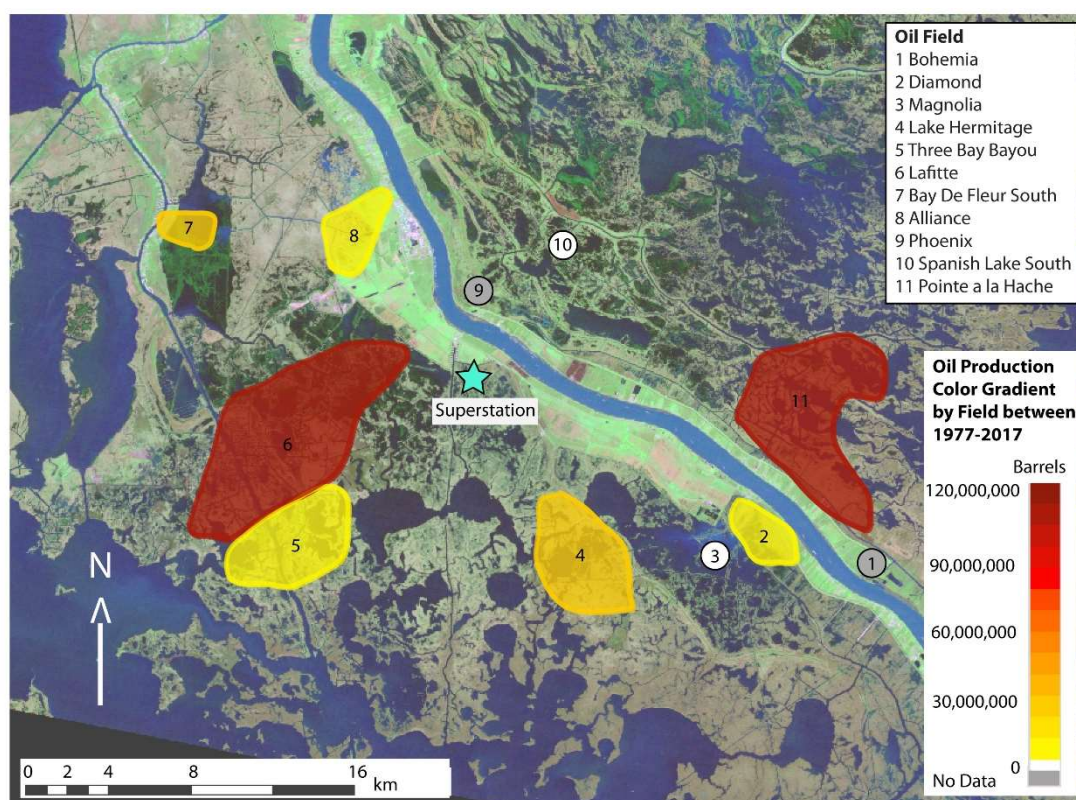
Figure 20 *Total oil and gas production numbers from fields surrounding the Superstation. Data are only available from 1977 to 2017 and two fields, Bohemia and Phoenix, had no production records for this time period. Data recovered from SONRIS, a Louisiana DNR database.*

The Superstation is not located near any faults that are known to have been active during the Holocene (Fig. 21) (Greene, 1998; Gagliano et al., 2003; Armstrong et al., 2014) but it does sit on the down-thrown side of the Ironton Fault which is ~4 km north of the Superstation. The Ironton fault has been identified previously in studies of the Lafitte oil field (Greene, 1998), but the eastern portion of the fault has not been published (Nancye

Dawers, personal communication, September 2017). This creates some uncertainty as to the potential effect of this normal fault on subsidence rates. Because the Ironton fault has not been traced through the Holocene (Greene, 1998; Nancye Drawers, personal communication, September 2017), it is assumed that it does not have a localized major effect on vertical displacement rates measured at the Superstation. Ongoing work to compile a Fault Atlas for Southern Louisiana with the use of 3D seismic data will potentially clarify the role of the Ironton fault but because most of this data is proprietary at this time, a more extensive analysis on the potential role of faulting at the site is currently not feasible.

Most of the compaction analysis is focused on the displacement measurements of sample Myrtle Grove I-2 and the M-O transition because their formation elevation can be linked to the tidal range. The other two samples (Myrtle Grove I-1 and I-3) provide minimum rates because they are from freshwater environments which can form at elevations significantly higher than sea level. Myrtle Grove I-1, the shallowest and youngest samples, has compacted at an average rate of 2.46 mm/yr (the minimum possible rate), the second highest rate of the three vertical displacement calculations. Myrtle Grove I-3 has the lowest average rates of compaction (0.85 mm/yr) but could be higher because this is a minimum rate. Despite being 0.8 m below Myrtle Grove I-2, I-3 has been vertically displaced only ~0.13 m more than I-2. These two samples are almost 900 years apart in age and because the peat has a very low bulk density (0.3-0.4 g/cm^3), it indicates that minimal compaction occurred during the deposition of the inter-subdelta peat.
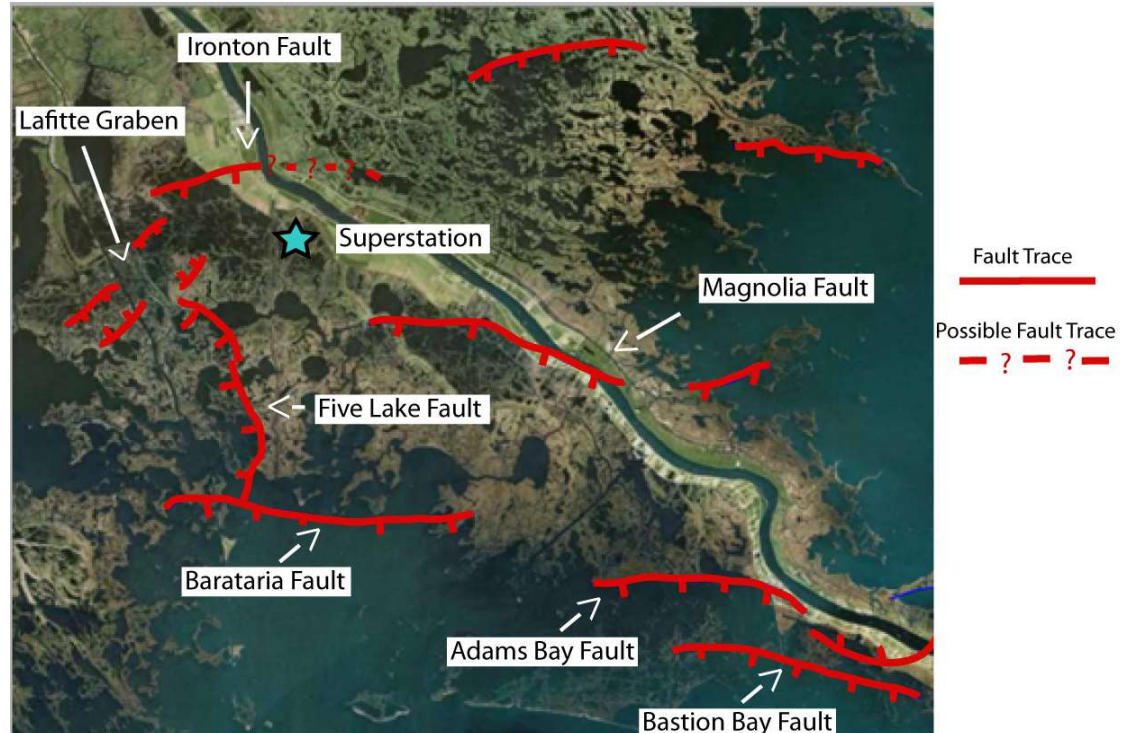
Figure 21 *Map of faults near the Myrtle Grove Superstation. The eastern tip of the Ironton Fault is unknown and is marked with a "-?-" trace. Traces are courtesy of Dr. Dawers of Tulane University and have previously been reported in Greene (1998), Gagliano et al. (2003), and Armstrong et al. (2013).*

Previous studies have shown that the amount of compaction is closely tied to overlying sediment type and thicknesses (e.g., Chamberlain, 2017). An example of this is the differential subsidence at the Superstation site caused by the crevasse-splay deposit that overlies the intercalated peat (Fig. 17). Because the deposit is thicker and coarser grained at the Superstation compared to the rest of the region, it can be assumed to have a higher bulk density (Table 3). Furthermore, if the peat beds are assumed to form as a level surface with minimal deviation in elevation (Törnqvist et al., 2008) then Myrtle Grove I-2 is calculated to have been compacted up to 2.36 m due to the additional loading of the thicker crevasse-splay deposit. This 2.36 m is the difference in compaction measured in the Myrtle Grove I core (5.14 m) and across the region (2.78 m). Because crevasse splays can be

erosive, the top of the inter-subdelta peat in the Myrtle Grove I core could have been eroded to a lower elevation than the surface at other parts in the region. This is supported by the unconformity at the top of the intercalated peat but this would imply that the thickness of the peat bed at the Superstation site should be smaller than the rest of the region which is not the case. Additional calculations can be done with the base of the peat, which is also assumed to have formed at a uniform elevation. The difference in elevation of the base of the peat between the Myrtle Grove I core and across the region is 1.88 m, so at a bare minimum, 1.88 m of the 2.36 m of vertical displacement measured at the top of the peat is due to compaction.

Present-day rates of shallow subsidence are measured through CRMS stations located across the MRD. CRMS station 0276, which is only 170 m from the Superstation, shows a rate of 0.4 mm/yr from 2008-2015 (Jankowski et al., 2017), which is most likely due to compaction. Myrtle Grove I peat and M-O derived rates are averaged over several thousand years (0.85-2.60 mm/yr, Table 10) which shows that there is a discrepancy between Holocene and modern rates of compaction. Because compaction occurs most rapidly in the top few meters (Kuecher, 1994), present-day rates would be expected to be higher than past rates, but this is not the case. Modeling of sediment compaction has shown that the highest rates of compaction are induced by rapid sediment loading (Meckel et al., 2006). Surrounding the Myrtle Grove site, the top ~1 m of sediment is an organic rich, low density (<0.3 g/cm^3) marsh that has caused almost no sediment loading (Fig. B.5). This means that the peat is generally uncompacted and is not inducing significant loading in the area which could explain why shallow subsidence rates are so low at the CRMS site. Further insight into deep and shallow subsidence rates will be provided by the recently

installed GPS and fiberoptic strainmeters at the Superstation. This instrumentation can provide sub-mm scale accuracy to subsidence rates at the Superstation site over three different depth intervals. Furthermore, this instrumentation will establish background subsidence rates for projects such as the planned Mid-Barataria sediment diversion, which will likely induce high rates of load-induced compaction.

Sediment diversions are designed to behave similarly to crevasse splays by diverting a portion of river flow and sediment through a designed breach in the levee in order to build land. This will rapidly increase sediment accretion and loading, increasing the vertical effective stress (σ'_v) and in turn, rates of compaction. By drawing a comparison at the Superstation with the Plaquemines-Modern crevasse splay (Fig. 17), deposition by the sediment diversion could induce several meters of compaction on a thousand year timescale, especially in areas with thicker sand deposits. In order for this to be quantified, soil compaction from a geotechnical perspective needs to be better understood.

5.4   Compaction Potential

Consolidation of sediment occurs in two stages, including primary consolidation and secondary compression. Primary consolidation represents the reduction in void space due to an increase in pressure, or loading. This change in void space is due to the expulsion of pore water. Primary consolidation ends when void pressure reaches equilibrium with the increased overburden pressure exerted from newly deposited sediment. Secondary compression starts after equilibrium is reached and is represented by the realignment of sediment grains. For a sand, this restructuring is relatively small but for a texture with

larger void spaces, such as peat, it is more significant (Das, 1990). C_c, or the compression index, measures the amount of consolidation that will occur for a normally consolidated sample (Das, 1990; Terzaghi et al., 1996). Samples CS-2 and CS-34 are overconsolidated, or have experienced a σ'_v greater than that of the current overlying sediment and the measured C_c values are lower, to some degree, than they would be if they were normally consolidated (Brain, 2015).

Compressibility is determined by the grain size, depositional environment, and minerology of the sediment. In the clay fraction (<2 μm), minerology is very important because of the different bonds and forces that form between particles. In other words, all 0-2 μm sized grains do not behave similarly, which affects how the sediment responds at different water contents, and in turn, it affects compressibility. These three factors are best described by Atterberg Limits which are defined by a set of standardized tests which describe sediment behavior. Liquid Limit (LL) and Plastic Index (PI), which are Atterberg Limits, can be used to estimate compressibility.

The six Holocene samples tested for their geotechnical properties are separated by lithogenetic units. CS-2 and CS-8 are overbank deposits and CS-2 is likely a crevasse-splay deposit. CS-10 is a mouth-bar deposit, CS-12 is a delta-front deposit, and 20 and 34 are from the prodelta. Generally, like deposits share similar consolidation properties. Because of the large variability in grain size distribution in the overbank deposits, they often show larger variability in consolidation properties than other lithogenetic units (Kuecher, 1994, Montgomery, 1974). This is observed when comparing the compressibility of CS-2 and CS-8, where C_c is 0.23 and 0.60, respectively. While CS-10 is from mouth-bar deposits, it was sampled from an interval with relatively low sand content (19.6%). Thus, it is likely

60

not representative of the mouth-bar deposit, which can possess a sand content of >90% (Fig. 11), and it is more compressible like the prodelta and delta-front samples. The prodelta and delta-front samples show compressibility and permeability properties that are similar to each other, although the delta-front, CS-12, is the least compressible because of the higher sand content (8% compared to 0.1%).

Table 11 Preconsolidated geotechnical characteristics of different lithogenetic units in the MRD (Kuecher, 1994). Atterberg limits were not determined for several facies because the sand content was too high. Water content calculated using engineering standards is included in parenthesis.

Lithogenetic Unit	C_C Value	Liquid Limit	Plastic Index	Water Content[1]
Marsh	4.72	N/A	N/A	86.4-88.4 (660-765%)
Prodelta	2.25-1.03	62-90%	39-50%	53.1-64.9 (113-185%)
Bay-mud	0.82	121-128%	70-76%	55.8-60.5 (126-153%)
Mouth-bar	0.23-0.12	N/A	N/A	20.6 (26%)
Overbank (Natural levee)	0.12	N/A	N/A	23.7 (31%)
Point bar	0.06	30-55%	N/A	18.7 (23%)
Beach	0.05	N/A	N/A	19.4 (24%)

Kuecher (1994) conducted a geotechnical investigation of MRD sediment by considering the properties of different lithogenetic units. Additional lithogenetic units were identified but do not correspond to any deposits described in the current study. They are included (Table 11) to show a range of possible values. Samples were taken from active depositional environments in the MRD which means they were collected from a depth <2 m. This is particularly important for organic-rich sediment because most compaction occurs in this interval (Kosters, 1989). In order to minimize volume loss during sampling, a liquid nitrogen annulus coring device was developed that froze the sample in-situ and

---

[1] Water content is calculated differently depending on the field of study. This paper primarily uses geologic methods but geotechnical values (water weight/dry weight) are included in parenthesis for comparison with other geotechnical studies.

then thawed it in the lab before testing (Kuecher, 1994). Seven different facies were tested and relevant values are listed in Table 11.

While samples from the Myrtle Grove I study could be matched to Kuecher (1994) based on lithogenetic unit interpretations, the Atterberg Limits generally did not agree with each other. For example, LL for the prodelta from the current study ranged from 46-47% whereas Kuecher (1994) LL were 62-90%. Because the depositional environment should be similar for prodelta deposits from both studies, the clay content and clay minerology must be different. This means that even within similar lithogenetic units, samples may not be comparable between different studies and that from a geotechnical standpoint, single values for lithogenetic units, may not be representative of the whole. An additional note is that Kuecher (1994) noted bioturbation in the larger, box-cored prodelta sample whereas this study's prodelta samples were well laminated which could explain some differences in results between these studies.

Another geotechnical study (Montgomery, 1974) compared geotechnical and sediment data from USACE borings collected from revetment construction sites between Donaldsonville and Head of Passes, LA. Deposits were broken into several lithogenetic units, including overbank (natural levee), prodelta, and interdistributary deposits. The only organic-rich deposits described in that study were backswamp deposits and based on their descriptions, they are not directly comparable to organic-rich deposits in the present study.

The geotechnical properties of deposits in the present study vary significantly from values in Montgomery (1974) (Table 12). For comparison of the present study with Montgomery (1974), CS-2 is identified as an overbank (natural-levee) deposit with a measured LL and C_c of 25.9% and 0.23, respectively. These values fall on the lower end

of the spectrum for natural-levee deposits in Table 12. CS-8 is an overbank deposit, which is identified in the Montgomery (1974) study. The LL (42.6%), w_c (30.24 %), PI (21.2%), and C_c (0.60) of CS-8 fall within the reported ranges of the interdistributary deposit although below the averages. CS-20 and 34, are prodelta deposits and each geotechnical characteristic falls within the range of values reported by Montgomery (1974) prodelta but are below the average value (compare Tables 7 and 12).

Table 12 *Average geotechnical characteristics of different deposits in the MRD reported by Montgomery (1974). Water content is calculated using geology and engineering methods, the latter of which in brackets. Average values are denoted by parenthesis.*

Deposit	Water Content %[2]	Liquid Limit	Plastic Index	Compressibility Index
Overbank (Natural Levee)	15.3-45.4 (31.0) [18-83 (45)]	29-129 (66)	2-90 (42)	0.25-2.75
Prodelta	23.7-41.2 (34.7) [31-70 (53)]	39-100 (79)	16-72 (51)	0.27-0.95
Interdistributary	19.4-57.1 (36.3) [24-133 (57)]	38-179 (82)	19-162 (59)	0.4-1.25

Comparisons with Kuecher et al. (1994) and Montgomery (1974) show that there is a large range of values for consolidation and Atterberg tests in the MRD. Reported values from the present study are not always similar to average values reported in Montgomery (1974) but generally fall in the lower ranges of w_c, LL, PI, and C_c. Due to the large range of values found in each lithogenetic unit, it is clear that compressibility can vary greatly between, and even within, deposits.

One potential application of the consolidation tests is to use them for modeling of compaction rates and to compare those with the measured rates from the Myrtle Grove I

---

[2] Water content is calculated differently depending on the field of study. This thesis primarily uses geologic methods but geotechnical values (water weight/dry weight) are included in brackets for comparison with other geotechnical studies.

core. This is beyond the scope of this thesis but could produce some valuable insight into the subsidence and settling history of the core. Without modeling, only a few observations can be made about which lithogenetic units are accommodating the most compaction. Our results support the general assumption that compaction occurs most in the deposits directly underlying the measured samples. For the M-O transition, vertical displacement is accommodated primarily in the delta-front and prodelta because the mouth bar itself has a low compressibility and for sample Myrtle Grove I-2, compaction is occurring in the inter-subdelta marsh, the overbank, delta-front, and prodelta deposits.

6. CONCLUSIONS

Stratigraphic analysis and dating of a 38.7 m core provides new insight into the depositional evolution of the Superstation study site. The top 12 m of the core contains both the Plaquemines-Modern and St. Bernard subdeltas and OSL dating of the St. Bernard mouth-bar sands show that the St. Bernard subdelta had prograded past the Superstation site as early as 3.7 ka. The central portion of the core contains 23 m of mud-dominated delta-front and prodelta deposits and the base of the core contains the top of the Pleistocene and a near-basal peat.

Comparison of dated facies boundaries and a relative sea-level curve for the MRD show that mean rates of compaction over the last two to four thousand years are as high as 2.60 mm/yr. This stands in contrast with present-day shallow subsidence rates of 0.4 mm/yr measured at a nearby CRMS site, which are likely due to the low amounts of mineral sediment loading and the very low bulk density of the accumulating marsh peat in this region. Despite these low current rates, mouth-bar sands have been vertically displaced up to 8.0 m mostly through the compaction of underlying delta-front and prodelta deposits, and inter-subdelta marshes have been displaced up to 6.0 m due to compaction of peats, overbank, delta-front, and prodelta deposits. Additionally, the Plaquemines-Modern crevasse-splay deposits show that thicker coarse-grained deposits will increase effective stress relative to finer-grained deposits and can induce differential compaction.

Geotechnical analysis of the Myrtle Grove I core provides consolidation testing results and Atterberg Limits for several different lithogenetic units. The results show that there are a wide range of potential values across the MRD for geotechnical properties and

that average geotechnical properties from other studies (i.e. Montgomery, 1974) may not

be representative of individual sites within the MRD.

APPENDIX A

A. OSL METHODS

A.1 Sample preparation

OSL sample preparation was performed under amber light conditions at Tulane University and at the Netherlands Centre for Luminescence dating (NCL). Bulk material was wet-sieved to isolate the 75-125 μm fraction, which was then chemically treated with 30% H_2O_2 to remove organics and 10% HCl to remove carbonates. The quartz fraction was isolated through density separation at 2.72 and 2.62 g/cm^3. This material was etched in 40% hydrofluoric acid (HF) for 40 minutes, rinsed with deionized water, treated with 10% HCl for 40 minutes, and rinsed again with deionized water. Quartz grains were adhered to stainless steel disks using silicon spray and masks of 1 mm or 5 mm diameter, depending on the test performed.

A.2 OSL measurement

Luminescence measurements were conducted at NCL using an automated Risø D15 TL/OSL reader. Blue (~470 nm) and infrared (~875 nm) light emitting diodes (LEDs) were used for optical stimulation and the heating element in the Risø reader was used for heating. The luminescence signals were detected through a 7.5 mm Hoya U-340 (U-340) filter with a UV detection window. The samples were irradiated with a $^{90}Sr/^{90}Y$ beta-source providing a dose rate of 0.085 ± 0.002 Gy/s.

OSL measurements were made for 20 s over 1000 channels. The luminescence signal was integrated over the first 0.48 s and the subtracted early background was

integrated over 0.48 -1.76 s to minimize the contribution of medium and slow components (Cunningham and Wallinga, 2010). Aliquot acceptance criteria included recycling and OSL infrared (IR) depletion ratios of 10% (Duller, 2003), a maximum test dose error of 20%, and recuperation of 5% relative to the natural signal.

Thermal transfer and dose recovery tests were conducted to inform and validate the protocol used for equivalent dose (D_e) extraction. The thermal transfer test was executed using 5 mm diameter aliquots (~1875 grains per disk), following Truelsen and Wallinga (2003). Based on the thermal transfer results (Fig. A.1), we selected a preheat temperature of 200 °C for subsequent equivalent dose (D_e) extraction.

D_es were obtained through the measurement of 1 mm diameter aliquots (~75 grains per disk) using a single-aliquot regenerative-dose (SAR) protocol (Murray and Wintle, 2000, 2003). The SAR protocol employed the 200 °C preheat, 180 °C cut heat, 4 regenerative points, one recuperation point, recycling checks including IR depletion of the OSL signal (Duller, 2003), and a 210 °C hot bleach. A dose recovery test using the same protocol and a dose of 2.13 ± 0.04 Gy given to 1 mm diameter aliquots returned a dose recovery ratio of 1.04 ± 0.04 (Fig. A.2), corroborating the SAR protocol.

A.3 Dose rate estimation

The natural radiation of the bulk sediment matrix was assessed from activity concentrations of ^{40}K and several radionuclides from the uranium and thorium series, measured on a gamma spectrometer at Tulane University (Table A.1). The dose rate conversion factors of Guérin et al. (2011) and beta dose attenuation factors of Mejdahl

(1979) were used. The cosmogenic contributions to the dose were calculated following Prescott and Hutton (1994). Internal dosing of 0.03 ± 0.02 Gy/ka was assumed. No external alpha contribution was included because etching removed the alpha-exposed outer layer of the sand grains. Dose rate attenuation due to water content (Aitken, 1985) was assessed by drying bulk sediment for each sample in a low temperature oven; 5% uncertainty was added to accommodate disturbances due to sampling and/or variations in water content during burial (Table A.1).

A.4 Age calculation

D_e datasets obtained through the SAR protocol were cleaned at 3 standard deviations (Chamberlain et al., submitted-a) to remove potential outliers prior to age modelling. The paleodoses were obtained through a bootstrap (Cunningham and Wallinga, 2012) minimum age model (Galbraith et al., 1999) with a sigma_b input of $6.9 \pm 2.2\%$ informed by Chamberlain et al. (submitted-b). OSL ages were calculated by dividing the bootMAM paleodoses by the dose rates presented in Table A.1. The ages are reported in ka relative to 2010 CE, with 1σ uncertainty.

FIGURES AND TABLES
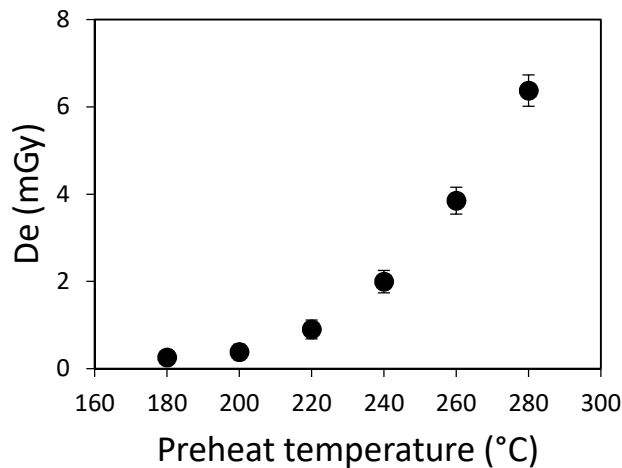
Figure A.122 *Results of the thermal transfer test, showing the average* D_e *of all OSL samples in this study (n=4) obtained by measuring zeroed sediments at increasing temperatures.*
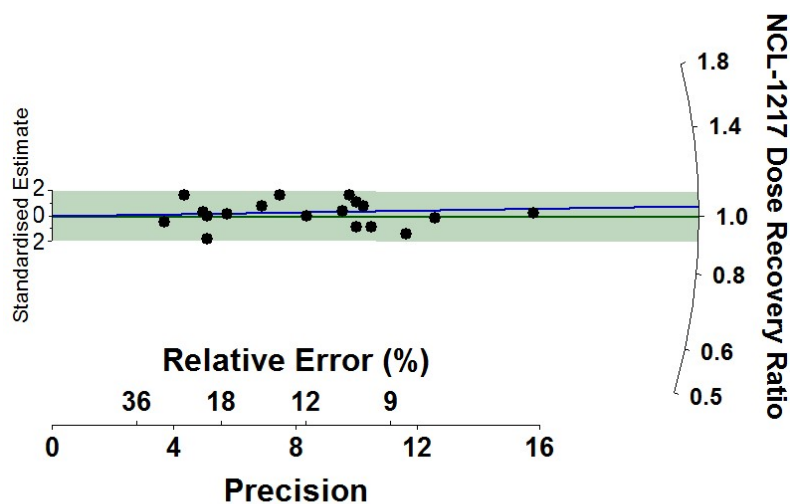
Figure A.223 *The dose recovery test of the four NCL-1217 quartz sand samples yielded a dose recovery ratio of 1.04 ± 0.04, with uncertainty reported as 1σ. The green line indicates unity and the blue line indicates the mean dose recovery ratio obtained through our measurement.*

Table A.13 *Details of OSL dose rate calculation, including water content, grain size, activities of isotopes derived from the uranium (U) and thorium (Th) chain and from potassium (^{40}K), the internal dose rate of quartz (Q internal), and the cosmogenic dose rate (D cosm.). The calculated dose rate (D), paleodose, and age relative to 2010 CE with 1σ uncertainty are given. All measurements were made on the 75-125 μm fraction of quartz sand.*

Sample name	Lab code	Depth (m)	Water content (%)	U (Bq/kg)	Th (Bq/kg)	40K (Bq/kg)	D cosm. (Gy/ka)	D (Gy/ka)	Paleo-dose (Gy)	Age (ka, 2010)
Myrtle Grove I-5	NCL-1217135	5.15-5.35	23 ± 5	35.03 ± 0.71	30.74 ± 0.48	565.55 ± 14.95	0.088 ± 0.009	2.38 ± 0.13	2.78 ± 0.23	1.25 ± 0.03
Myrtle Grove I-7	NCL-1217136	10.00-10.10	32 ± 5	41.16 ± 0.81	38.22 ± 0.55	607.03 ± 15.91	0.038 ± 0.004	2.28 ± 0.11	7.67 ± 0.51	3.36 ± 0.28
Myrtle Grove I-8	NCL-1217137	10.50-10.60	25 ± 5	41.38 ± 0.81	35.38 ± 0.52	567.42 ± 14.93	0.035 ± 0.004	2.40 ± 0.13	8.91 ± 0.46	3.71 ± 0.28
Myrtle Grove I-6	NCL-1217138	9.61-9.66	26 ± 5	32.99 ± 0.66	29.68 ± 0.45	545.38 ± 14.32	0.041 ± 0.004	2.14 ± 0.10	6.60 ± 0.67	3.07 ± 0.35

APPENDIX B

Figure 24 *– Myrtle Grove I hand core (ID # 601792-001) shell hash and top of the inter-subdelta peat at a depth of 6.30-6.60 m. Tape measurer corresponds to depth.*


Figure 252 *– Myrtle Grove I core immediately above the near basal wood peat with ~10 cm of humic clay and ~10 cm of silty clay at a depth of 36.7 to 37.0 m. White specks are small pieces of wax and tape measure does not correlate to depth.*

Figure 26 *Myrtle Grove I core delta-front deposit. Sediment textures are silty clay with silt laminations recovered from a depth of 12.61-12.84 m. Sample was split with a knife leaving diagonal artifacts across the sample face.*

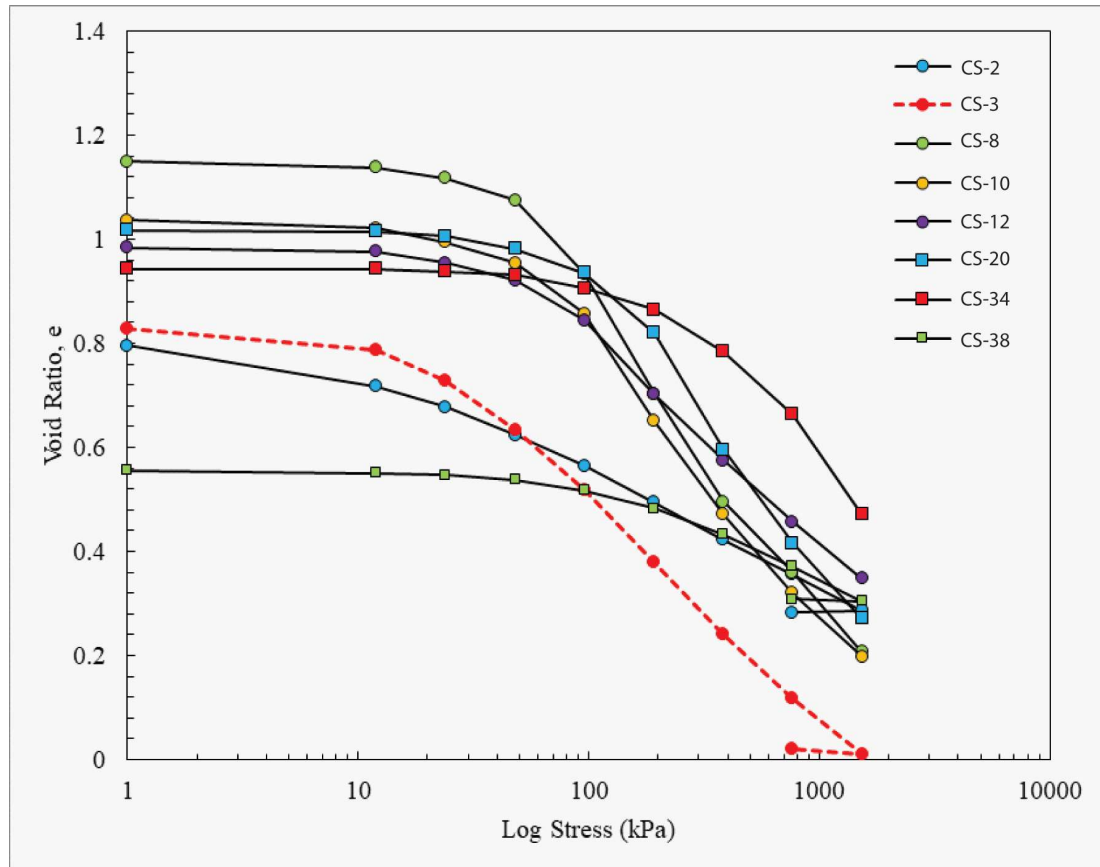**Figure 27** *Myrtle Grove I core prodelta deposit. Sediment texture is silty clay and was recovered from a depth of 18.02-18.19 m. Core was split with a knife leaving diagonal artifact across the core face.*
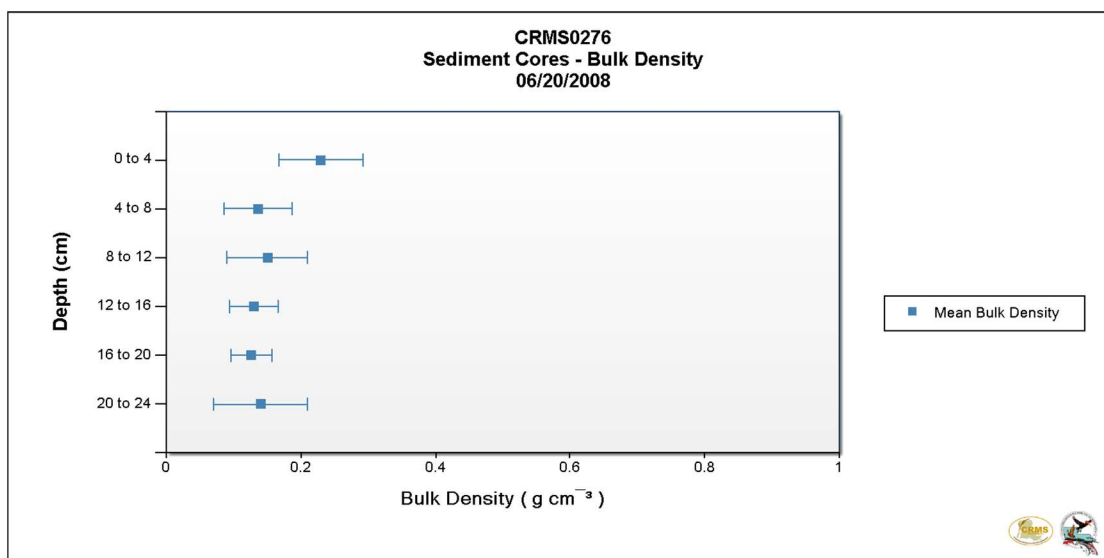
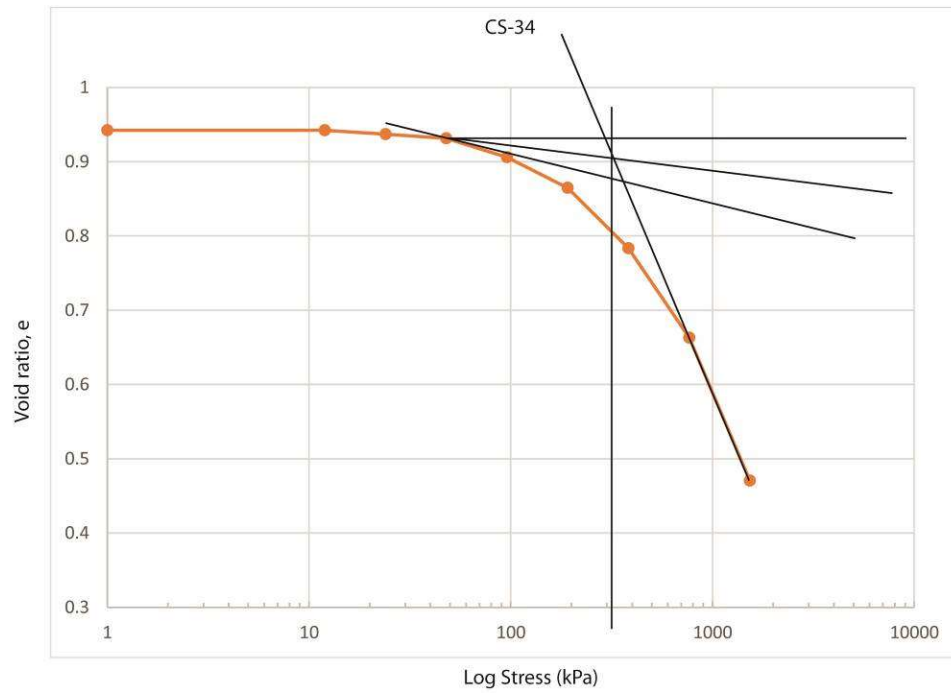***Figure 285*** *Bulk density measurements of the brackish marsh at CRMS 0276.*
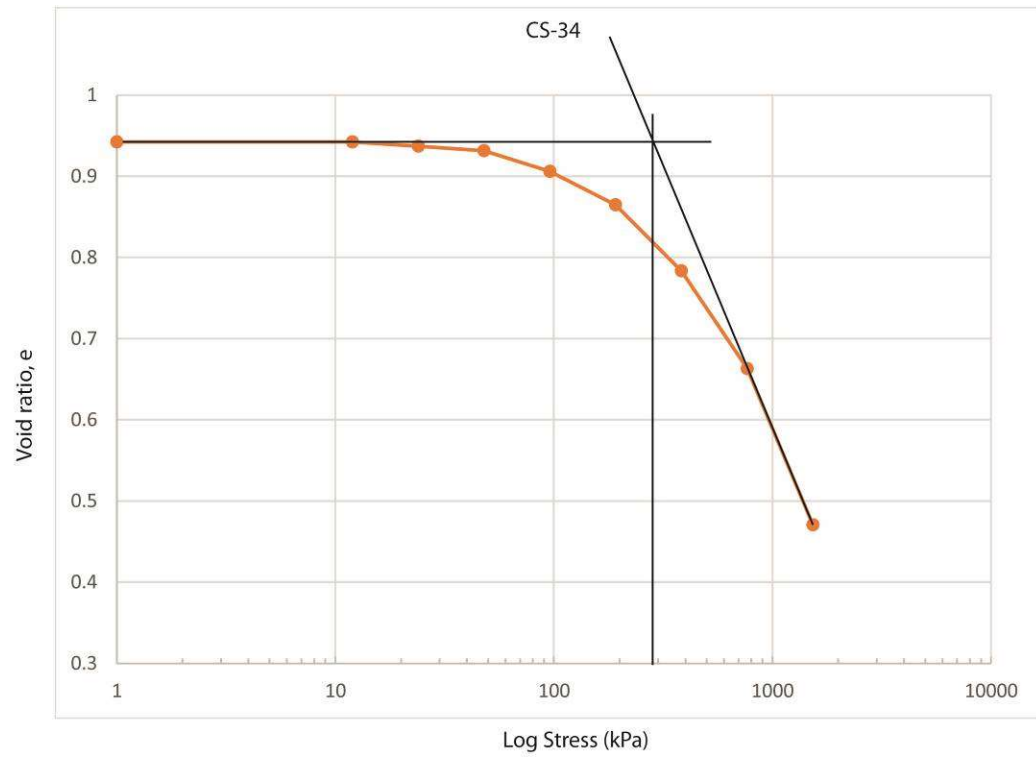
APPENDIX C

Figure C.1 *Log stress-e plots for eight samples from the Myrtle Grove I core including the excluded samples CS-3.*

Figure C.2 *Preconsolidation pressure estimate using Casagrande (1936) methods for CS-*

34

Figure C.3 *Preconsolidation pressure estimate using Sowers (1970) methods for CS-34.*

List of References

Adamiec, G., and Aitken, M., 1998, Dose-rate conversion factor: update: Ancient TL, v. 16, no. 2, p. 37–50.

Allison, M., Yuill, B., Törnqvist, T., Amelung, F., Dixon, T.H., Erkens, G., Stuurman, R., Jones, C., Milne, G., Steckler, M., Syvitski, J., and July, P.T., 2016, Global Risks and Research Priorities for Coastal Subsidence: Eos, Transactions American Geophysical Union, , no. 97, p. 22–27.

Armstrong, C., Mohrig, D., Hess, T., George, T., and Straub, K.M., 2014, Influence of growth faults on coastal fluvial systems: Examples from the late Miocene to Recent Mississippi River Delta: Sedimentary Geology, v. 301, p. 120–132, doi: 10.1016/j.sedgeo.2013.06.010.

ASTM International, 2017a, ASTM D2435 Standard Test Methods for One-Dimensional Consolidation Properties of Soils Using Incremental Loading: ASTM International, West Conshohocken, PA

ASTM International, 2017b, ASTM D4318-17 Standard Test Methods for Liquid Limit, Plastic Limit, and Plasticity Index of Soils.: ASTM International, West Conshohocken, PA.

ASTM International, 2017c, D2487-11 Standard Practice for Classification of Soils for Engineering Purposes (Unified Soil Classification System): ASTM International, West Conshohocken, PA.

Blum, M.D., and Roberts, H.H., 2012, The Mississippi Delta Region: Past, Present, and Future: Annual Review of Earth and Planetary Sciences, v. 40, no. 1, p. 655–683, doi:

10.1146/annurev-earth-042711-105248.

Brain, M., 2015, Compaction, *in* Handbook of Sea-Level Research: John Wiley & Sons, p. 452–567.

Bronk Ramsey, C., 1995, RADIOCARBON CALIBRATION AND ANALYSIS OF STRATIGRAPHY : THE OxCal PROGRAM, *in* Cook, G.T., Harkness, D.D., Miller, B.F., and Scott, E.M. eds., Radiocarbon, p. 425–430.

Carnec, C., and Fabriol, H., 1999, Monitoring and modeling land subsidence at the Cerro Prieto geothermal field , Baja California , Mexico , using SAR interferometry: Geophysical Research Letters, v. 26, no. 9, p. 1211–1214.

Chamberlain, E.L., 2017, Dating Deltas [Ph.D Thesis]: Tulane University, New Orleans, p. 27-164.

Chang, C., Mallman, E., and Zoback, M., 2014, Time-dependent subsidence associated with drainage- induced compaction in Gulf of Mexico shales bounding a severely depleted gas reservoir: AAPG Bulletin, v. 98, no. 6, p. 1145–1159, doi: 10.1306/11111313009.

Chmura, A.G.L., Aharon, P., Chmura, G.L., and Aharont, P., 1995, Stable Carbon Isotope Signatures of Sedimentary Carbon in Coastal Wetlands as Indicators of Salinity Regime: Journal of Coastal Research, v. 11, no. 1, p. 124–135.

Couvillion, B.R., Barras, J.A., Steyer, G.D., Sleavin, W., Fischer, M., Beck, H., Trahan, N., Griffin, B., and Heckman, D., 2011, Land area change in coastal Louisiana (1932 to 2010): , p. 529.

Das, B.M., 1990, Principles of Geotechnical Engineering: PWS-KENT Publishing Company.

Dokka, R.K., 2011, The role of deep processes in late 20th century subsidence of New Orleans and coastal areas of southern Louisiana and Mississippi: Journal of Geophysical Research, v. 116, p. 1–25, doi: 10.1029/2010JB008008.

Gagliano, S.M., Kemp, E.B., Wicker, K.M., and Wiltenmuth, K.S., 2003, Active Geological Faults and Land Change in Southeastern Louisiana: A Study of Contribution of Faulting to Relative Subsidence Rates, Land Loss, and Resulting Effects on Flood Control, Navigation, Hurricane Protection and Coastal Restoration Projects. Coa.:

Glew, J.R., Smol, J.P., and Last, W.M., 2002, Sediment core collection and extrusion, *in* Tracking environmental change using lake sediments, Springer, p. 73–105.

González, J.L., and Tornqvist, T.E., 2006, Coastal Louisiana in crisis: Subsidence or sea level rise? Eos, Transactions American Geophysical Union, v. 87, no. 45, p. 493, doi: 10.1029/2006EO450001.

González, J.L., and Törnqvist, T.E., 2009, A new Late Holocene sea-level record from the Mississippi Delta: evidence for a climate/sea level connection? Quaternary Science Reviews, v. 28, no. 17–18, p. 1737–1749, doi: 10.1016/j.quascirev.2009.04.003.

Greene, A.L., 1998, Successful Utilization of 3D Seismic at Lafitte Field South Louisiana: 3-D Seismic Case Histories From the Gulf Coast Basin: Gulf Coast Association of Geological Societies, p. 159–171.

Haslett, S.K., Davies, P., Currf, R.H.F., Davies, C.F.C., Kennington, K., King, C.P., Margetts, A.J., 1998, Evaluating late-Holocene relative sea-level change in the Somerset Levels , southwest Britain: The Holocene, v. 8, no. 2, p. 197–207.

Heiri, O., Lotter, A.F., and Lemcke, G., 2001, Loss on ignition as a method for estimating organic and carbonate content in sediment: reproducibility and comparability of results: NatureJournal of Paleolimnology, v. 25, p. 101–110, doi: 10.1017/CBO9781107415324.004.

Hijma, M., Engelhart, S., Törnqvist, T., Horton, B., Hu, P., and Hill, D., 2015, A protocol for a geological sea-level database, *in* Shennan, I., Long, A., and Horton, B. eds., Handbook of Sea-Level Research, Wiley Blackwell, p. 536–553.

Hijma, M.P., Shen, Z., Törnqvist, T.E., and Mauz, B., 2017, Late Holocene evolution of a coupled , mud-dominated delta plain – chenier plain system , coastal Louisiana , USA: Earth Surface Dynamics, v. 5, no. 4, p. 689–710, doi: 10.5194/esurf-2017-24.

Jankowski, K.L., Törnqvist, T.E., and Fernandes, A.M., 2017, Vulnerability of Louisiana's coastal wetlands to present-day rates of relative sea-level rise: Nature Communications, , no. 8, p. 1–7, doi: 10.1038/ncomms14792.

Jones, C.E., An, K., Blom, R.G., Kent, J.D., Ivins, E.R., and Bekaert, D., 2016, Anthropogenic and geologic influences on subsidence in the vicinity of New Orleans, Louisiana: Journal of Geophysical Research: Solid Earth, v. 121, p. 3867–3887, doi: 10.1002/2015JB012636.Received.

Kesel, R., Yodis, E., and McCraw, D., 1992, An approximation of the sediment budget of the lower Mississippi River prior to major human modification: Earth Surface

Processes and Landforms, v. 17, p. 711–722.

Kolker, A.S., Allison, M.A., and Hameed, S., 2011, An evaluation of subsidence rates and sea-level variability in the northern Gulf of Mexico: Geophysical Research Letters, v. 38, no. 21, doi: 10.1029/2011GL049458.

Kuecher, G.J., 1994, Geologic Framework and Consolidation Settlement Potential of the Lafourche Delta , Topstratum Valley Fill ; Implications for Wetland Loss in Terrebonne and Lafourche Parishes , Louisiana [Ph.D. Thesis]: Louisiana State University, Baton Rouge, 27-58 p.

Louisiana Coastal Protection and Restoration Authority, 2017, Restoration Authority of Louisiana (CPRA)(2017). Louisiana's Comprehensive Master Plan for a Sustainable Coast: p. 190

Louisiana Natural Hertiage Program, and Louisiana Department of Wildlife and Fisheries, 2009, The Natural Communities of Louisiana: http://www.wlf.louisiana.gov/wildlife/natural-communities (accessed January 2018).

Meckel, T.A., ten Brink, U.S., and Williams, S.J., 2006, Current subsidence rates due to compaction of Holocene sediments in southern Louisiana: Geophysical Research Letters, v. 33, no. 11, doi: 10.1029/2006GL026300.

Mesri, G., and Ajlouni, M., 2007, Engineering Properties of Fibrous Peats: Journal of Geotechnical and Geoenvironmental Engineering, v. 133, no. 7, doi: 10.1061/(ASCE)1090-0241(2007)133.

Montgomery, R.L., 1974, Correlation of Engineering Properties of Cohesive Soils

Bordering the Mississippi River from Donaldsonville to Head of Passes, LA: No. WES-MP-S-74-20. Army Engineer Waterways Experiment Station Vicksburg, MS.

Morton, R. a., and Bernier, J.C., 2010, Recent Subsidence-Rate Reductions in the Mississippi Delta and Their Geological Implications: Journal of Coastal Research, v. 26, no. 3, p. 555–561, doi: 10.2112/JCOASTRES-D-09-00014R1.1.

Morton, R.A., and White, W.A., 1997, Characteristics of and Corrections for Core Shortening in Unconsolidated Sediments: Journal of Coastal Research, v. 13, no. 3, p. 761–769.

Murray, A.S., and Wintle, A.G., 2000, Luminescence dating of quartz using an improved single- aliquot regenerative-dose protocol: Radiation Measurements, v. 32, no. 1, p. 57–73, doi: 10.1016/S1350-4487(99)00253-X.

Nummedal, D., and Swift, D.J.P., 1987, Transgressive stratigraphy at sequence-bounding unconformities: some principles derived from Holocene and Cretaceous examples: Sea level fluctuation and coastal evolution, v. 41, p. 241–260, doi: 10.2110/pec.87.41.0241.

Olson, R.E., and Daniel, D.E., 1981, Measurement of the Hydraulic Conductivity of Fine-Grained Soils: Permeability and groundwater contaminant transport, ASTM International.

Peel, F., Travis, C., and Hossack, J., 1995, Genetic structural provinces and salt tectonics of the Cenozoic offshore US Gulf of Mexico; a preliminary analysis: Salt Tectonics, AAPG Memoir 65, v. 65, p. 153–175.

Plaquemines Parish, 2014, Coastal protection and restoration (section 6) *in* Plaquemines Parish Comprehensive Master Plan: http://plaqueminesparish.com/wp/wp-content/uploads/2015/02/Coastal_Protection_and_Restoration_Assessment_2012521 3237.pdf (accessed January, 2018)

Roberts, H.H., 1997, Dynamic Changes of the Holocene Mississippi River Delta Plain: The Delta Cycle: Journal of Coastal Research, v. 13, no. 3, p. 605–627, doi: 10.2307/4298659.

Roberts, H.H., Bailey, A., and Kuecher, G.J., 1994, Subsidence in the Mississippi River Delta-Important influences of valley filling by cyclic deposition, primary consolidation phenomena, and early diagenesis: Transactions of the Gulf Coast Association of Geological Societies, v. 44, p. 619–629.

Terzaghi, K., Peck, R.B., and Mesri, G., 1996, Soil mechanics in engineering practice: John Wiley & Sons, New York.

Törnqvist, T.E., González, J.L., Newsom, L.A., Borg, K. Van Der, Jong, A.F.M. De, and Kurnik, C.W., 2004, Deciphering Holocene sea-level history on the U . S . Gulf Coast : A high-resolution record from the Mississippi Delta: GSA Bulletin, v. 116, no. 7, p. 1026–1039, doi: 10.1130/B2525478.1.

Törnqvist, T.E., Kidder, T.R., Autin, W.J., van der Borg, K., de Jong, A.F.M., Klerks, C., Snijders, E., Storms, J.E.A., van Dam, R.L., and Wiemann, M.C., 1996, A Revised Chronology for Mississippi River Subdeltas: Science, v. 273, p. 1693–1696.

Törnqvist, T.E., Wallace, D., Storms, J., Wallinga, J., van Dam, R., Blaauw, M., Kersen, M., Klerks, C., Meijneken, C., and Snijders, E., 2008, Mississippi Delta subsidence

primarily caused by compaction of Holocene strata: Nature Geoscience, , no. 1, p. 173–176.

USDA, 1999, Soil Taxonomy. A Basic System of Soil Classification for Making and Interpreting Soil Surveys: USDA and NRCS Agriculture Handbook Number 436, Washington, DC.

Vetter, L., Rosenheim, B., Fernandez, A., and Törnqvist, T., 2017, Short organic carbon turnover time and narrow 14C age spectra in early Holocene wetland paleosols: Geochemistry, Geophysics, Geosystems, v. 18, no. 1, p. 142–155.

Wellner, R., Beaubouef, R., Van Wagoner, J., Roberts, H., and Sun, T., 2005, Jet-Plume Depositional Bodies--The Primary Building Blocks of Wax Lake Delta: The Gulf Coast Association of Geological Societies, v. 55, p. 867–909.

Wolstencroft, M., Shen, Z., Törnqvist, T.E., Milne, G.A., and Kulp, M., 2014, Understanding subsidence in the Mississippi Delta region due to sediment, ice, and ocean loading: Insights from geophysical modeling: Journal of Geophysical Research: Solid Earth, , v. 119, no. 4, p. 3838–3856, doi: 10.1002/2013JB010928.

Yu, S.Y., Törnqvist, T.E., and Hu, P., 2012, Quantifying Holocene lithospheric subsidence rates underneath the Mississippi Delta: Earth and Planetary Science Letters, v. 331–332, p. 21–30, doi: 10.1016/j.epsl.2012.02.021.

BIOGRAPHY

Jonathan G. Bridgeman grew up and lived most of his life in Solvang, California where he learned to explore creation. The rolling hills of the Santa Ynez Valley and the numerous adventures in nature with his family sparked in him an interest to study at the University of California, Los Angeles. He then moved to New Orleans, Louisiana to study the Mississippi River and coastal processes at Tulane University with Torbjörn Törnqvist. Jon hopes to continue working on coastal issues and use what he's learned to help communities adapt to rapidly changing landscapes and environments.